Unveiling the reaction mechanism of the N(^{2}D) + pyridine reaction: ring-contraction versus 7-membered ring formation channels

Luca Mancini,[a] Gianmarco Vanuzzo,[a] Pedro Recio,[a] Adriana Caracciolo,[a] Noelia Faginas-Lago,[a,b] Marzio Rosi[c,d], Piergiorgio Casavecchia[a,d]*, and Nadia Balucani[a,]*

[a]*Dipartimento di Chimica Biologia e Biotecnologie, Università degli Studi di Perugia, 06123 Perugia, Italy*

[b]*Master-Tec Srl, 06128 Perugia, Italy*

[c]*Dipartimento di Ingegneria Civile e Ambientale, Università degli Studi di Perugia, 06125 Perugia, Italy*

[d]*Computational Laboratory for Hybrid/Organic Photovoltaics (CLHYO), Istituto CNR di Scienze e Tecnologie Chimiche "Giulio Natta" (CNR-SCITEC), 06123 Perugia, Italy*

ABSTRACT: Despite the relevance of the reactions of the prototypical nitrogen-containing six-membered aromatic molecule (N-heterocyclic) of pyridine (C_6H_5N) in environmental science, astrochemistry, planetary science, prebiotic chemistry, and material science, few experimental/theoretical studies exist on the bimolecular reactions involving pyridine and neutral atomic/molecular radicals. We report a combined experimental and theoretical study on the elementary reaction of pyridine with excited nitrogen atoms, N(^{2}D), aimed at providing information on the primary reaction products and their branching fractions (BFs). From previous crossed molecular beam (CMB) experiments with mass-spectrometric detection and present synergistic calculations of the reactive potential energy surface (PES) and product BFs we have unveiled the reaction mechanism. It is found that the reaction proceeds *via* N(^{2}D) barrierless addition to pyridine that, *via* bridged intermediates followed by N atom "sliding" into the ring, leads to 7-membered ring structures. They further evolve, mainly *via* ring-contraction mechanisms toward 5-membered ring radical products and, to a smaller extent, *via* H-displacement mechanisms toward 7-membered ring isomeric products and their isomers. Using the theoretical statistical estimates, an improved fit of the experimental data previously reported has been obtained leading

to the following results for the dominant product channels: C_4H_4N (pyrrolyl) + HCN (BF = 0.61 ± 0.20), $C_3H_3N_2$ (1H-imidazolyl/1H-pyrazolyl) + C_2H_2 (BF = 0.11 ± 0.06), and $C_5H_4N_2$ (7-membered ring molecules or pyrrole carbonitriles) + H (BF = 0.28 ± 0.10). The ring-contraction product channels C_4H_4N (pyrrolyl) + HCN, $C_3H_3N_2$ (1H-imidazolyl) + C_2H_2, $C_3H_3N_2$ (1H-pyrazolyl) + C_2H_2, and C_5H_5 (cyclopentadienyl) + N_2 have statistical BFs of 0.54, 0.09, 0.11, and 0.07, respectively. Among the H-displacement channels, the cyclic-CHCHCHCHNCN + H channel and cyclic-CHCHCHCHCN$_2$ + H are theoretically predicted to have a comparable BF (0.07 and 0.06, respectively), while the other isomeric 7-membered ring molecule + H channel has a BF or 0.03. Pyrrole-carbonitriles and 1H-ethynyl-1H-imidazole (+ H) isomeric channels have an overall BF = 0.03. Implications for the chemistry of Saturn's moon Titan and prebiotic chemistry, as well as for understanding the N-doping of graphene or carbon nanotubes, are noted.

∗**Corresponding authors**: Piergiorgio Casavecchia (piergiorgio.casavecchia@unipg.it); Nadia Balucani (nadia.balucani@unipg.it);

Keywords: Nitrogen atom reactions with aromatics/heterocyclic – Molecular beam reaction dynamics – Materials science – Atmospheric chemistry of Titan

1. INTRODUCTION

Pyridine, the simplest azarene with gross formula C_5H_5N, is largely used as an intermediate for the manufacture of bioactive products, such as medicines, herbicides, insecticides, and fungicides.[1] While it is not abundant in nature, its derivatives are part of important biomolecules such as niacin (Vitamin B_3), pyridoxine (a form of vitamin B_6), and nicotinamide adenine dinucleotide.[2-5] Some pyridine derivatives were identified in carbonaceous chondrites and also in the pristine sample of the carbonaceous asteroid (162173) Ryugu collected by the Hayabusa2 mission.[6] Its derivative nicotinonitrile (3-cyanopyridine) is one of the molecules synthesized in a version of the Stanley-Miller experiment with C_2H_4/NH_3 mixtures.[7] Because of that and considering that it is an organic molecule simple enough to be synthesized in abiotic processes, it has been searched also in the interstellar medium and in the atmosphere of Titan (the massive moon of Saturn) where a plethora of N-containing organic molecules have been already identified.[8] In the case of Titan, the presence of protonated pyridine and pyrimidine was speculated by the analysis of the mass spectra recorded by the Ion Neutral Mass Spectrometer (INMS) onboard the Cassini spacecraft,[9] but ground-based attempts to verify that by using the ALMA telescope could not confirm its presence and only upper limits were derived.[10] Nonetheless, polycyclic aromatic hydrocarbons (PAHs) and N-containing PAHs (N-heterocyclic compounds and aromatic amines) have been invoked[11] to explain the strong unidentified emission near 3.28 μm recorded by Dinelli et al.[12] In addition, the analysis of the data recorded by the Cassini Plasma Spectrometer Ion Beam Spectrometer (CAPS-IBS) strongly suggests that PAHs and N-containing PAHs are responsible for the heavy positive ion signal recorded at 170–310 Da.[13] PAHs and NPAHs are also considered as the carriers of the unidentified spectral bands (namely, the diffuse interstellar bands and the unidentified infrared bands) detected in several regions of the interstellar medium,[14] but neither pyridine nor any other individual N-containing aromatic compounds have been identified in the interstellar medium, and only upper limits for pyridine abundance were reported in C-rich circumstellar envelopes to date.[15] Several pyridine formation routes in both cold and hot extraterrestrial environments have been proposed[16-21] and, therefore, its missing detection suggests the presence of efficient destructive processes that deplete gaseous C_5H_5N.[22] For instance, in O-rich environments, the reaction with atomic oxygen is efficient in degrading it with the main products being pyrrole and CO.[23] In the upper atmosphere of Titan, an important active species that could consume pyridine, as well as other aromatic

compounds, is atomic nitrogen in its first excited state ^{2}D. N(^{2}D) can be formed by various N_2 dissociation processes, including extreme ultra-violet (EUV) photolysis, but also dissociative photoionization, dissociation via electron impact, galactic cosmic ray absorption, and N_2^+ dissociative recombination (see Ref. 24 and references therein). The ^{2}D state is metastable with radiative lifetimes of 13.6 and 36.7 hours for $^2D_{3/2}$ and $^2D_{5/2}$, respectively,[25,26] and is known to be very reactive with saturated and unsaturated aliphatic hydrocarbons[27-35]as well as with nitriles,[36-38] water[39,40] and H_2/D_2.[41,42]

Until recently, not much was known on the reactivity of N(^{2}D) with aromatic compounds. In a recent paper, a combined experimental and theoretical study on the reaction N(^{2}D) + benzene was reported.[43] Experimentally, the reaction was studied under single-collision conditions by the crossed molecular beams (CMB) scattering method with mass spectrometric detection (MS) and time-of-flight (TOF) analysis and in a continuous supersonic flow reactor. The global rate constant as a function of temperature from 50 K to 296 K and the product branching fractions (BFs) were determined.[43] In addition, electronic structure calculations of the reactive potential energy surface (PES) were performed, and the product BFs were also determined via RRKM/ME (Rice-Ramsperger-Kassel-Marcus/Master Equation) estimates.[43] The absence of an entrance barrier in the derived PES corroborated the experimental data on the rate coefficients which were found to be in the gas-kinetic range (ca. 2×10^{-10} cm^3 s^{-1}) over the 50–296 K range of temperatures investigated. Experimental and theoretical BFs agree in identifying the ring-contraction channel leading to C_5H_5 (cyclopentadienyl) and HCN to be largely dominant.[43]

Another reason to pursue the study of N(^{2}D) reactions with aromatic compounds is to understand the N-doping of graphene or carbon nanotubes via the use of plasma. N-doped graphene is an interesting material for electrocatalysis and biosensing applications.[44-46] According to the data available, N-doped graphene includes graphitic N atoms (with the nitrogen atom in the graphene plane), pyridinic N and pyrrolic N atoms.[44-46] Among the different methods to dope graphene, the nitrogen plasma treatment is a simple approach that allows efficient material surface modification.[44-46] Nitrogen plasma can be produced either in low pressure radiofrequency/microwave discharges or at ambient pressure in electrical discharges (see Ref. 47 and references therein). While the doping mechanism at the atomistic level remains largely unknown, a more detailed characterization of the dielectric barrier discharge method has clearly indicated the role of neutral nitrogen and, in particular, of the ^{2}D and ^{2}P excited electronic states

of atomic nitrogen.[47] Further investigation[48] revealed that the reactions of N(^{2}D,^{2}P) with the cation of toluene are able to form bridged intermediates of the same kind we have found for the reaction N(^{2}D) + C_6H_6.[43] From that bridged structure, the N atom "slides" into the ring forming a 7-membered structure that can then evolve further.

In a recent Letter we reported the results of a CMB study of the title reaction at a collision energy (E_c) of 33.5 kJ/mol with a preliminary analysis of the experimental data.[49] From the data analysis, we were able to identify two main groups of product channels: a group of channels associated with H-displacement mechanisms accompanied by the formation of a variety of isomeric $C_5H_4N_2$ co-products, and a group associated with the formation of two heavy co-products, corresponding to ring-contraction mechanisms and elimination of HCN and/or C_2H_2, CN, and N_2. Since the resolution in determining the product translational energy was not good enough to distinguish among isobaric products, we could not provide detailed BFs. Nevertheless, from the backward-forward symmetric shape of the product angular distributions, it resulted quite clearly that the reactive system behaves statistically.[49] This has motivated us to pursue a theoretical characterization of the PES and of RRKM BFs, in spite of the difficulties expected after the work done for N(^{2}D) + C_6H_6 and in consideration of the symmetry loss in the case of pyridine.

Here, we report quantum chemical calculations of the $C_5H_5N_2$ PES as well as RRKM/ME computations of the product BFs at the collision energy of the CMB experiment and as a function of temperature. The theoretical work warranted an improved analysis of the earlier CMB experimental data and a reconsideration of the global product BFs.

From the combined experimental/theoretical results a clearer picture of the N(^{2}D) + pyridine reaction mechanism, including the product channel distribution, has emerged. Overall, the approach is the same that we employed for the investigation of a variety of reactions between N(^{2}D) and saturated[29,30] and unsaturated aliphatic hydrocarbons,[33-35] simple nitriles,[36-38] as well as benzene.[43]

The paper is organized as follows. Sections 2 and 3 describe the theoretical and experimental methods, respectively. Section 4 presents the theoretical results, while section 5 summarizes the improved analysis of the earlier experimental data and the comparison with the theoretical predictions. Discussion follows in section 6 and Conclusions are given in section 7.

2. THEORETICAL METHODS

2.1. Electronic structure calculations of the potential energy surface. The $N(^2D)$ + C_5H_5N reaction PES was investigated adopting a well-established computational strategy previously used for the characterization of similar bimolecular reactions.[34-36,43,50-52] In detail, the lowest stationary points (minima and transition states) were located at the B3LYP[53,54] level of theory, in conjunction with the 6-311+G(d,p) basis set.[55,56] The optimization of the stationary points was then refined using the same hybrid density functional with a larger basis set, *i.e.*, the Dunning correlation consistent valence polarized aug-cc-pVTZ basis set.[57-59] Harmonic vibrational frequencies were computed at the same level of theory in order to check the nature of the stationary points, *i.e.* minimum if all the frequencies are real, saddle point if there is one, and only one, imaginary frequency. Intrinsic reaction coordinate (IRC) calculations[60,61] were performed to assign the identified saddle points. All the energies were corrected to 0 K by adding the zero-point-energy (ZPE) correction computed using the scaled harmonic vibrational frequencies, evaluated at the B3LYP/aug-cc-pVTZ level. The energy of $N(^2D)$ was estimated by adding the experimental[62] separation $N(^4S)$–$N(^2D)$ of 230 kJ/mol to the energy of $N(^4S)$ at all levels of calculation. Furthermore, the exothermicity of the main product channels, which were demonstrated to be relevant from RRKM calculations, was evaluated performing more accurate calculations at the CCSD(T) level corrected with a Density Fitted (DF) MP2 extrapolation to the complete basis set (CBS) and with corrections for core electron excitations. In particular, the energies were computed as:

$$E_{CBS}= E(CCSD(T)/aug\text{-}cc\text{-}pVTZ)+[E(CCSD(T,core)/cc\text{-}pVTZ)-E(CCSD(T)/cc\text{-}pVTZ)]+[E(DF\text{-}MP2/CBS)-E(DF\text{-}MP2/aug\text{-}cc\text{-}pVTZ)]$$

where E(DF-MP2/CBS) is defined as:

$$E(DF\text{-}MP2/CBS) = E[(DF\text{-}MP2)/aug\text{-}cc\text{-}pVQZ]+0.5772*[E(DF\text{-}MP2/aug\text{-}cc\text{-}pVQZ)-E(DF\text{-}MP2/aug\text{-}cc\text{-}pVTZ)]$$

The E(DF-MP2/CBS) extrapolation was performed using Martin's two parameter scheme.[63]

Since the accuracy of our best computed values should not be better than the "chemical accuracy" of 1 kcal/mol (4.184 kJ/mol), we rounded all the reported energies to 1 kJ/mol. All DFT calculations were performed using Gaussian 09[64] while the CBS calculations were performed using MOLPRO.[65,66] The analysis of the vibrational frequencies was performed using Avogadro.[67]

2.2. Statistical estimates of the product branching fractions (BFs). Statistical RRKM calculations for the N(^{2}D) + C_5H_5N reaction were carried out using a code implemented in our group for this purpose.[36,50-52,68] The microcanonical rate constant *k(E)* for a specific reaction, at a specific total energy, is given by the expression[69] $k(E) = \frac{N_{TS}(E)}{h\rho(E)}$ where $N(E)$ represents the sum of states of the transition state at energy E, $\rho(E)$ is the density of states of the reactants, and h is Planck's constant. $N(E)$ is obtained by integrating the relevant density of states (DOS) up to energy E, and the rigid rotor/harmonic oscillator model is assumed. Where possible, tunneling (as well as quantum reflection) was included in the RRKM calculations using the corresponding imaginary frequency of the transition state and calculating the tunneling probability for the corresponding Eckart barrier. For the cases in which we were not able to locate a clear transition state in the exit channel, the corresponding microcanonical rate constant was obtained through a variational approach: $k(E)$ was evaluated at various points along the reaction coordinate and the point which minimizes the rate constant was chosen, in accordance with the variational theory.[70] In some cases, however, that approach could not be employed because of some difficulties in the electronic structure calculations of the intermediate points, and the transition state was assumed as the products at infinite separation. After the calculation of all microcanonical rate constants, a Markov (stochastic) matrix was set up for all intermediates and final channels to derive the product branching fractions for the overall reaction. Finally, a Boltzmann averaging allowed us to obtain the branching fractions for each product channel as a function of temperature.

RRKM/ME calculations were carried out individually for initial intermediates resulting from the addition of N(^{2}D) to pyridine in our PES. We have identified, indeed, six possible intermediates, all formed without an entrance barrier according to our calculations (see Figure 1; see also Figure S1 of the Supplementary Information for the scan of the entrance channels pointing to absence of a barrier for those approaches). In cases like this, it is not easy to estimate the global value of the product BFs because it is not possible to establish how the initial reaction flux is distributed among the initial intermediates. In a purely statistical approach, however, we can assume that the initial association process between the reactants is partitioned between the various

intermediates based on their DOS, calculated considering their relative energy (that is, the well depths associated with them) and the values of vibrational frequencies and rotational constants. The rotational densities of states were calculated using an inverse Laplace transform of the corresponding partition functions. Subsequently, a convolution between the rotational densities of states and the corresponding vibrational ones was performed using a direct count algorithm.

The strong assumption here is that, when the two reactants start interacting in the long-range potential region, the system already behaves statistically.

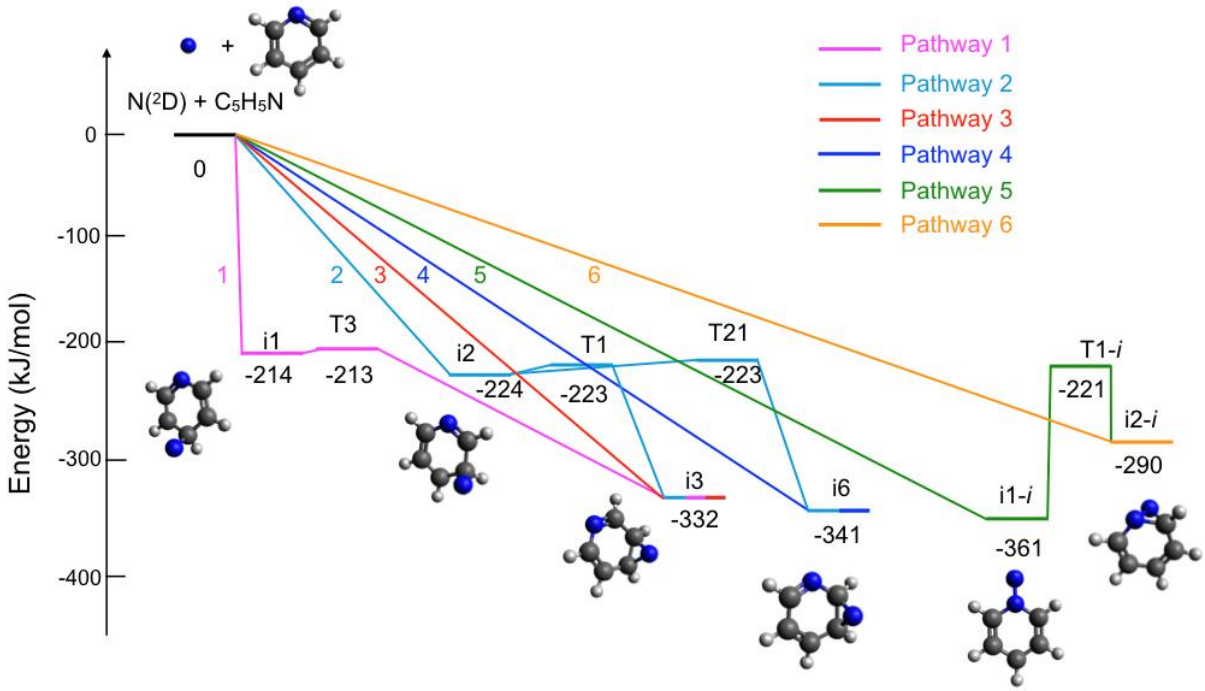

Figure 1. The entrance channel of the global PES for the N(^{2}D) + C_5H_5N reaction. Six different pathways have been identified leading to six different addition intermediates (B3LYP/aug-cc-pVTZ level of theory) (see text).

3. EXPERIMENTAL METHOD

The details of the CMB experiment were reported in our previous Letter.[49] Briefly, using a CMB apparatus described elsewhere,[71-74] two continuous supersonic beams of the reactants were crossed at 90^o under single-collision conditions in a large scattering chamber kept at 1.5×10^{-6} mbar in operating conditions. The detector (a tunable electron impact ionizer followed by a quadrupole

mass filter and a Daly type ion detector) can be rotated in the plane of the reactants and a chopper wheel can be used to measure the TOF distributions of the reactants (using the single-shot configuration) and products (using the pseudorandom configuration). The atomic nitrogen beam was produced by a radio-frequency discharge source where high dissociation (about 60%) of N_2 is achieved. Atomic nitrogen, produced in a distribution of electronic states, was characterized in our laboratory by Stern-Gerlach magnetic analysis.[75] 72% of N atoms are in the ^4S ground state, while 21% and 7% in the metastable excited states ^2D and ^2P states, respectively. The presence of N(^4S) and N(^2P) in the beam does not affect our experiments as already observed in the other reactions that we have investigated with the same source. Details on the experimental conditions and beam production can be found in Ref. 49. The experimental collision energy, E_c, and the center-of-mass angle, Θ_{CM}, were 33.5 kJ/mol and 66.5°, respectively.

Product angular distributions, $N(\Theta)$, were measured in the laboratory (LAB) reference frame by modulating at 160 Hz the pyridine beam for background subtraction. Product TOF distributions were measured by the pseudo-random chopping method at 6 μs/channel. Pivotal to the success of the experiments has been the use of soft-ionization at 17 eV electron energy to suppress or mitigate interferences from dissociative ionization processes of reactants, products and background gases.[71,76] In this kind of experiments, quantitative information is obtained by moving from the LAB coordinate system to the center-of-mass (CM) one and analyzing the best-fit product angular, $T(\theta)$, and translational energy, $P(E'_T)$, distributions into which the total CM product flux, $I_{CM}(\theta, E'_T)_{total}$, can be factorized.[71] The best-fit CM functions are derived by a forward convolution fit of the total product LAB angular and TOF distributions. When at a certain mass-to-charge ratio (*m/z*) value we observe the contributions from more than one channel, the convolution routine makes use of the equation $I_{CM}(\theta, E'_T)_{total} = \sum_i w_i [T(\theta) \times P(E'_T)_i]$, where the w_i parameters represent the relative contribution of the apparent integral cross section of the i^{th} channel and are determined during the best-fit procedure.[71,76] The w_i parameters enter in the evaluation of the product channel BFs, as described elsewhere.[71]

In our previous Letter, during the data analysis we were only able to disentangle two groups of reaction channels: the H-displacement channels and the ring-contraction channels. Because of the low resolution and unfavorable kinematics, we could not distinguish among the possible isomeric co-products in the H-displacement channels nor the almost isobaric co-products of the

$HCN/C_2H_2/CN/N_2$ formation channels. Here, a more detailed analysis of the experimental distributions guided by the theoretical BFs is presented (see below).

4. THEORETICAL RESULTS

4.1. Potential energy surface. The characterization of the PES has been a daunting task due to the different possible attacks in the *ortho*, *meta*, *para*, and *ipso* positions and bridge additions. Also, the first intermediates formed following the initial addition steps can isomerize to many other intermediates before reaching the exit channels. Indeed, as already observed for the $N(^2D)$ + benzene reaction,[43] the large input energy provided by the electronically excited atomic nitrogen and the ability of N and C to form three and four bonds, respectively, lead to a notable number of possible rearrangements, all accessible because the involved transition states are below the total energy associated with the asymptote of the reactants. To reduce the cost the calculations, a preliminary scrutiny of the PES was performed at the B3LYP/6-311+G(d,p) level of theory. Many different pathways were identified in this first screen, but some of them are obviously not competitive (and, therefore, are expected to be minor) because of the presence of very high transition states and/or numerous rearrangements before reaching the product exit channel. For this reason, we carried out RRKM calculations to identify the reaction pathways that give a non-negligible contribution and for them we repeated the calculations at the more accurate B3LYP/aug-cc-pVTZ level of theory. Finally, the enthalpy changes of the main channels were recalculated at the very accurate CBS level. RRKM calculations of the BFs were also repeated considering the more accurate energy of the stationary points along the relevant reaction channels. The structure (in terms of cartesian coordinates) of the stationary points identified in the PESs are reported in the Supporting Information (Table S1).

As already mentioned six initial intermediates have been identified upon the $N(^2D)$ attack to the pyridine ring. All of them are formed without an entrance barrier, as in the case of the similar $N(^2D)$ + C_6H_6 reaction.[43] In Figure 1 a close-up of the entrance channel of the global PES is illustrated. The addition of $N(^2D)$ in the *para* position (pathway 1 in the Figure 1) leads to the formation of the i1 intermediate which is located 214 kJ/mol below the reactant energy asymptote. By overcoming a very small barrier (associated with transition state T3), i1 easily isomerizes to i3 (located at –332 kJ/mol) which is characterized by the presence of a 3-membered ring in a bridged

structure. The i3 intermediate can also be formed directly by bridge addition of N(^{2}D) to carbon atoms at the *meta* and *para* positions (pathway 3). The addition of N(^{2}D) in the *meta* position (pathway 2 in the Figure 1) leads to the formation of the i2 intermediate which is located 224 kJ/mol below the reactant energy asymptote. By overcoming very small barriers (associated with T1 and T21), i2 easily isomerizes to i3 or to i6 (located at –341 kJ/mol), another intermediate characterized by the presence of a 3-membered ring in a bridged structure. The i6 intermediate can also be formed directly by bridge addition of N(^{2}D) to carbon atoms at the *ortho* and *meta* positions (pathway 4). It should be noted that, with our calculations, we were unable to identify a structure similar to i1 and i2 but with the nitrogen atom added in the *ortho* position. Any attempt in this direction has always led to the i6 bridged structure upon optimization. This result may indicate that the structure formed by addition at the *ortho* position is not stable or that any transition state prior to its isomerization to i6 is so small that it cannot be computationally identified because of the convergence to the i6 structure when performing optimization. We have tested numerous other DFT methods without being able to isolate that structure. As a matter of fact, also the i1 and i2 intermediates have to overcome very small barriers of *ca.* 1 kJ/mol to isomerize into the corresponding bridged structures, but those were sufficient to allow the identification of their structures upon optimization. The lack of an *ortho*-addition intermediate and the very small isomerization barriers for i1 and i2 pose other problems on how to handle the different initial intermediates for RRKM estimates of BFs (see below). Finally, N(^{2}D) can add also at the *ipso* position forming the i1-*i* intermediate (–361 kJ/mol) that holds a N-N σ bond (pathway 5). By overcoming a barrier of 140 kJ/mol, i1-*i* can isomerize to i2-*i*, another intermediate characterized by the presence of a 3-membered ring in a bridged structure. Also in this case, i2-*i* can be formed directly by bridge addition of N(^{2}D) to carbon atoms at the *ipso* and *ortho* positions (pathway 6).

After these initial steps, many possible reaction pathways can occur. Here we will comment and further inspect only those pathways that make an appreciable contribution to the most significant reaction channels (see Figures 2-4) according to our RRKM calculations. Other pathways that we were able to identify along the PES (but which do not contribute significantly) are shown in Figures S2–S5 of the Supporting Information for completeness.

Once formed (either in pathways 1, 2 or 3), the i3 intermediate can isomerize to i4 (located 454 kJ/mol below the energy of the reactants), a 7-membered ring species with two nitrogen atoms in the ring (see Figure 2). The associated transition state, T4, (+10 kJ/mol with respect to i3) clearly

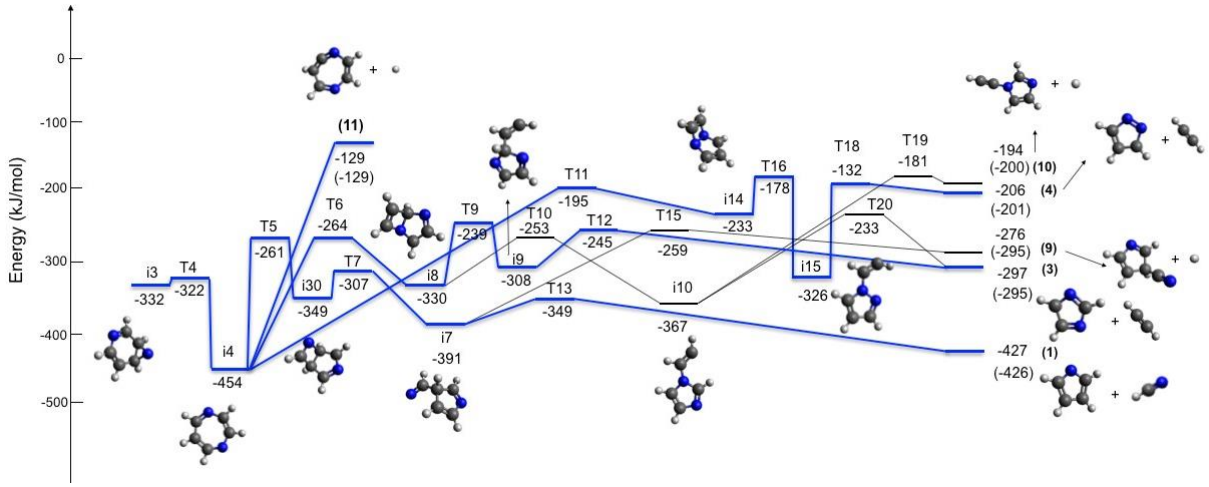

Figure 2. The main reaction pathways originating from the i3 intermediate (B3LYP/aug-cc-pVTZ level of theory) (see text). Values in parentheses of channel exothermicities are at CCSD(T)/CBS level of theory.

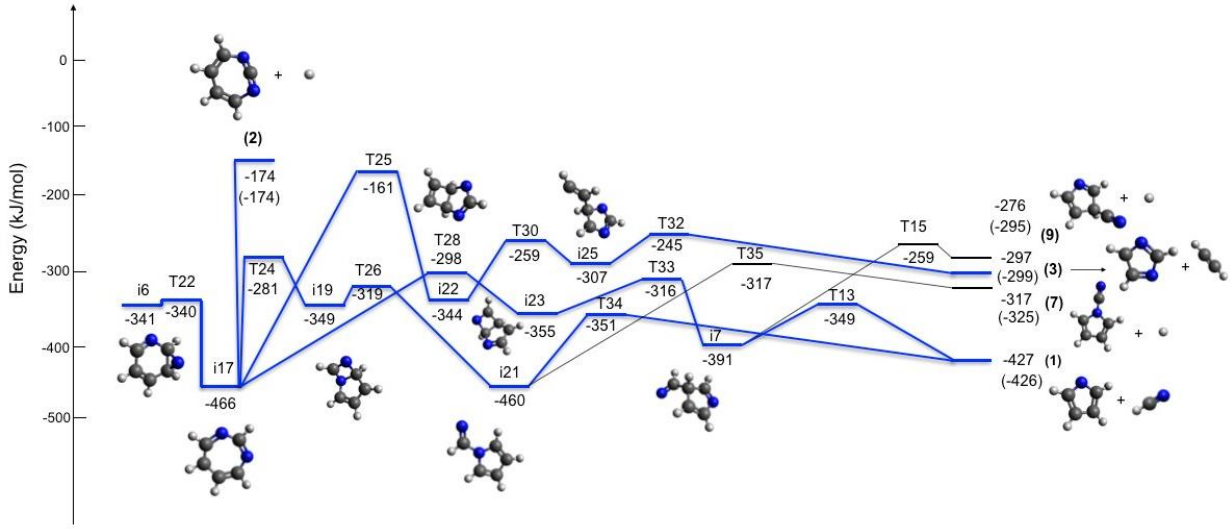

Figure 3. The main reaction pathways originating from the i6 intermediate (B3LYP/aug-cc-pVTZ level of theory) (see text). Values in parentheses of channel exothermicities are at CCSD(T)/CBS level of theory.

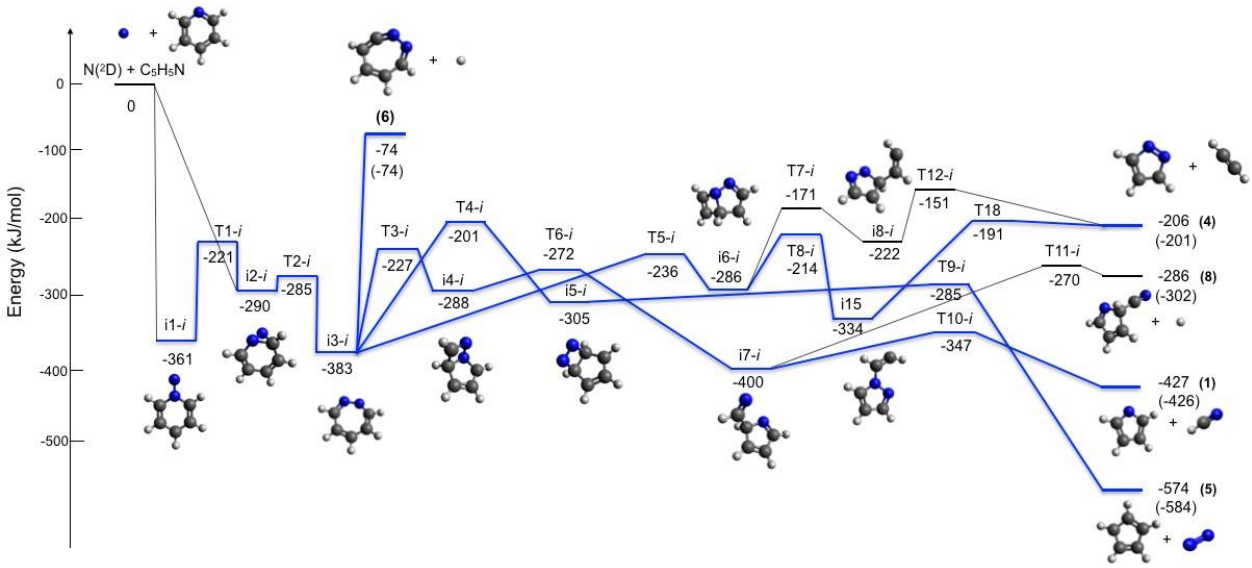

Figure 4. The main reaction pathways originating from the i1-*i* and i2-*i* intermediates (B3LYP/aug-cc-pVTZ level of theory) (see text). Values in parentheses of channel exothermicities are at CCSD(T)/CBS level of theory.

shows the breaking of a C-C bond that allows the N atom to "slide" into the ring. In turn, the i4 intermediate can directly dissociate to the products of channel (11), one of the H-displacement mechanisms. The calculated enthalpy change of channel (11) is –129 kJ/mol. Alternatively, i4 can follow the path T5 → i30 → T7 → i7→ T13, leading to the products pyrrolyl radical (C_4H_4N) + hydrogen cyanide (HCN) (channel (1)). Additionally, a different isomerization path, T6 → i8 → T9→ i9→ T12, is responsible for the formation of the 1H-imidazolyl radical and acetylene (channel (3)). The global reaction enthalpy of the two product channels (1) and (3) are –427 kJ/mol and –297 kJ/mol, respectively, at the B3LYP/aug-cc-pVTZ level of theory.

On the other hand, whether formed in pathways 2 or 4, the i6 intermediate isomerizes to i17 (located 466 kJ/mol below the reactant energy asymptote), another 7-membered ring species with two N-atoms in the ring formed via the fission of a C-C bond and the "sliding" of the N-atom into the ring (a small barrier represented by T22 is easily overcome – see Figure 3). The 7-membered ring i17 intermediate can isomerize to i23 and then to i7 leading ultimately to the already described pyrrolyl + HCN product channel (1) through the path T28 → i23 → T33→ i7→ T13. A different exit channel from i17 is represented by H-loss with formation of the product channel (2) (ΔH^0_0= –174 kJ/mol) in a barrierless fashion (see Figure 3). A competing H-loss channel starting from i17 is associated with the C_4H_4N-CN (1-cyano-N-cyclopentadiene) co-fragment (channel (7)),

accessible via the path i17 →T24 → i19 → T26→ i21→ T35. Other possible product channels, originating from different isomerization processes, are characterized by the formation of C_4NH_4CN (3-cyano-N-cyclopentadiene) + H (channel (9) (see Figures 2 and 3)), C_3H_3NN-CCH + H (channel (10) (see Figure 2)), and 1H-pyrazolyl + C_2H_2 (channel (4) (see Figures 2 and 4).

Finally, i2-*i* (whether formed directly or by the isomerization of i1-*i* in pathways 5 and 6) easily evolves toward another 7-membered ring intermediate (i3-*i*) by overcoming a barrier of 5 kJ/mol associated with T2-*i* (see Figure 4). Once formed, the i3-*i* intermediate can directly dissociate, leading to the formation of H + cyclic-CHCHCHCHCN$_2$ (another 7-membered ring species) (channel (6)) in a barrier-less process. Alternatively, several isomerization processes can take place. Formation of pyrrolyl + hydrogen cyanide products (channel (1)) is possible through the path T3-*i* → i4-*i* → T6-*i* → i7-*i* → T10-*i*. Alternatively, a ring contraction channel leading to the elimination of molecular nitrogen and the formation of cyclopentadienyl (C_5H_5) radical (channel (5)) is possible via the sequence T4-*i* → i5-*i* → T9-*i*. This is the most exothermic channel of the global PES with a ΔH^0_0 of –574 kJ/mol at this level of theory. Another pathway originating from i3-*i* leads to the formation of 1H-pyrazolyl + acetylene (channel (4)), through the T5-*i* → i6-*i* → T8-*i* → i15 → T18 reaction path. The i15 intermediate is a species which is formed also in pathways 1, 2, and 3 (see Figure 2). Finally, another H-loss channel leading to the C_4NH_4CN (pyrrole-2-carbonitrile) co-fragment (channel (8)) (see Figure 4), starting from i7-*i* is possible (from i6-*i* there is also a higher energy path to channel (4) via T7-*i* → i8-*i* → T12-*i*).

In conclusion, from our electronic structure calculations of the global PES, we have identified the 11 main exothermic product channels which are listed below (a 12th channel is also considered because in our previous analysis of the experimental results we considered a CN formation channel):

$N(^2D) + C_5H_5N$	→ C_4H_4N(pyrrolyl) + HCN	ΔH^0_0= –426 kJ/mol (1)
	→ cyclic-CHCHCHCHNCN + H	ΔH^0_0= –174 kJ/mol (2)
	→ $C_3H_3N_2$(1H-imidazolyl) + C_2H_2	ΔH^0_0= –299 kJ/mol (3)
	→ $C_3H_3N_2$(1H-pyrazolyl) + C_2H_2	ΔH^0_0= – 201 kJ/mol (4)
	→ C_5H_5(cyclopentadienyl) + N_2	ΔH^0_0= –584 kJ/mol (5)
	→ cyclic-CHCHCHCHCN$_2$ + H	ΔH^0_0= –74 kJ/mol (6)
	→ C_4H_4N-CN(1H-pyrrole-1-carbonitrile) + H	ΔH^0_0= –325 kJ/mol (7)

$\rightarrow C_4NH_4$-CN(2H-pyrrole-2-carbonitrile) + H ΔH^0_0= –302 kJ/mol (8)

$\rightarrow C_4NH_4$-CN(3H-pyrrole-3-carbonitrile) + H ΔH^0_0= –295 kJ/mol (9)

$\rightarrow C_4NH_3N$-CCH(1H-ethynyl-1H-imidazole) + H ΔH^0_0= –200 kJ/mol (10)

$\rightarrow$ cyclic-CHCHNCHCHCN + H ΔH^0_0= –129 kJ/mol (11)

$\rightarrow C_4H_5N$ (3H-pyrrole) + CN ΔH^0_0= –229 kJ/mol (12)

While the channel notation is the same used in the Figures 2-4, here the reaction enthalpies are those obtained at the more accurate CCSD(T)/CBS level of theory (these values are in parentheses in the Figures 2-4). As visible, there is reasonable agreement with the B3LYP/aug-cc-pVTZ values (with the largest deviation being *ca*. 20 kJ/mol), thus corroborating the choice of the method to derive the entire PES. The reason why the reaction enthalpies for some channels differ up to about 20 kJ/mol can be due to correlation effects, which are better taken in account in the case of CCSD(T)/CBS calculations

The structures of the main molecular products are shown in Figure 5.

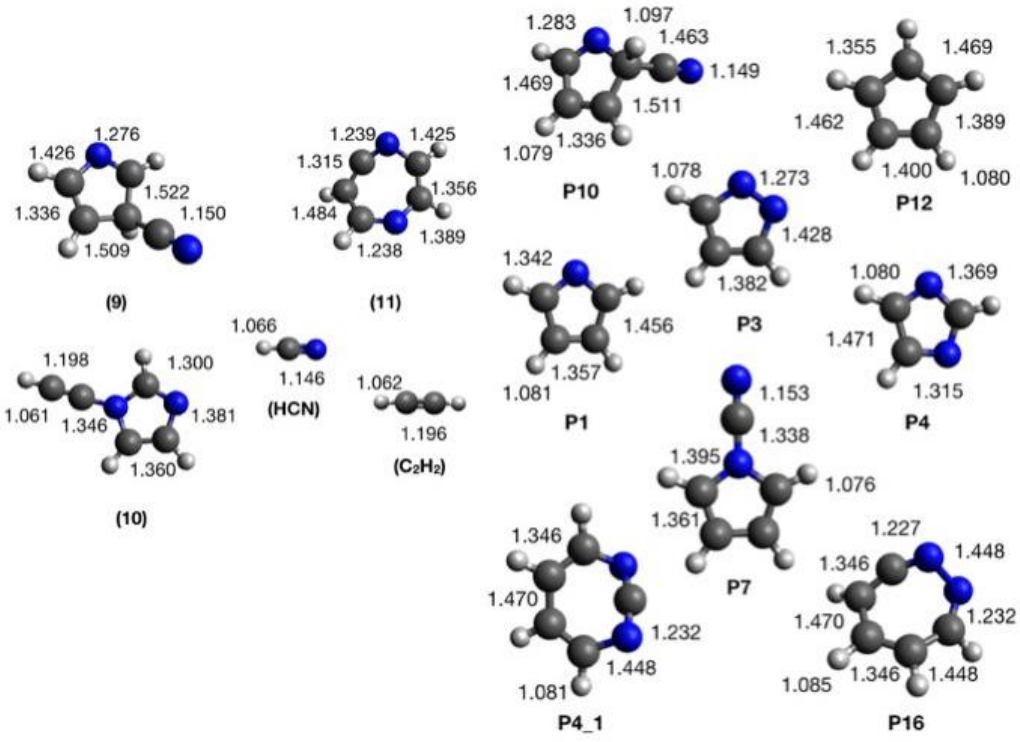

Figure 5. Structure of main reaction products evaluated at the B3LYP/aug-cc-pVTZ level of theory. Distances in Å.

In addition to the five ring-contraction channels and seven H-displacement channels, abstraction of an H atom by N(^{2}D) is also possible, forming NH and three different (*ortho*, *meta*, and *para*) pyridinyl radicals C_5H_4N. These channels are calculated at the CBS level to be exothermic by 114, 95, and 89 kJ/mol for *o*-, *m*-, and *p*-attack, respectively. We were unable to locate a transition state for the H-abstraction, even though the presence of an entrance barrier is expected. To be noted that in the related system O(^{1}D) + benzene, a submerged transition state was located for the analogous H-abstraction mechanism.[77] Despite that, the calculated BF for the H-abstraction mechanism was found to be minor (confirmed by the experimental results).[77]

Overall, the PES obtained for the N(^{2}D) + C_5H_5N reaction is similar in many aspects to the one developed for the N(^{2}D) + C_6H_6 reaction.[43] Because of the symmetry loss due to the presence of a nitrogen atom in the structure of pyridine, the global $C_5H_5N_2$ PES is much more complex and a larger number of reaction pathways and product channels are present.

4.2. RRKM/ME estimates of the product branching fractions. RRKM estimates of product BFs were performed at the collision energy of the CMB experiment[49] and for two different temperatures, 200 K and 300 K, corresponding to the temperature of Titan's atmosphere at 1000 km of altitude (where the molar fraction of N(^{2}D) has its peak)[78] and room temperature, respectively. The calculated BFs refer to the zero-pressure limit, which nicely simulates the conditions of the CMB experiments and is a good approximation of the very low pressure of the thermosphere of Titan. The RRKM approach allows the calculations of unimolecular processes (isomerizations and dissociations) of reaction intermediates. Three sets of independent calculations were carried out starting from the intermediates i3, i6 and i2-*i* because (*i*) i1 and i2 promptly isomerize to i3 and i6 because T2 and T1/T21 are degenerate with their minima and (*ii*) the only destiny of i1-*i* is to isomerize to i*2*-i. In the Tables 1-3 the channel specific BFs are reported at the CMB E_c and for T = 50, 200 and 300 K (the values at 50 K are shown to see the possible trend by decreasing the available energy).

In all cases and under all considered conditions, the dominant channel is the one leading to C_4H_4N(pyrrolyl) + HCN (channel (1)) with a BF varying from 0.614 (i3), 0.687 (i6), and 0.583 (i2-*i*) at 50 K to 0.545 (i3), 0.558 (i6), and 0.538 (i2-*i*) under the conditions of the CMB experiment. The second channel by importance when starting from i3 and i6 is the 1H-imidazolyl + C_2H_2 channel (3) with BFs of 0.254 (i3) and 0.197 (i6) at 50 K that decrease to 0.239 (i3) and 0.173 (i6) under CMB conditions. Channel (3) is minor in the case of the i2-*i* PES portion where, instead, the

Table 1. Theoretical channel-specific product BFs for the N(^{2}D) + C_5H_5N reaction at three temperatures (50 K, 200 K, and 300 K) and at E_c= 33.5 kJ/mol, starting from the i3 intermediate.

Product channel	ΔH^0_0 (kJ/mol)	Channel number	T = 50 K	T = 200 K	T = 300 K	E_c = 33.5 kJ/mol
C_4H_4N(pyrrolyl) + HCN	–426	1	0.614	0.598	0.572	0.545
$C_3H_3N_2$(1H-pyrazolyl) + C_2H_2	–201	4	0.021	0.023	0.023	0.031
$C_3H_3N_2$(1H-imidazolyl) + C_2H_2	–299	3	0.254	0.252	0.252	0.239
C_4NH_4CN + H	–295	9	0.016	0.016	0.016	0.019
C_3H_3NN-CCH + H	–200	10	0.011	0.011	0.011	0.018
cyclic-CHCHNCHCHCN + H	–129	11	0.083	0.100	0.126	0.148

Table 2. Theoretical channel-specific product BFs for the N(^{2}D) + C_5H_5N reaction at three temperatures (50 K, 200 K, and 300 K) and at E_c= 33.5 kJ/mol, starting from the i6 intermediate.

Product channel	ΔH^0_0 (kJ/mol)	Channel number	T = 50 K	T = 200 K	T = 300 K	E_c = 33.5 kJ/mol
C_4H_4N(pyrrolyl) + HCN	–426	1	0.687	0.596	0.581	0.558
$C_3H_3N_2$(1H-imidazolyl) + C_2H_2	–299	3	0.197	0.195	0.195	0.173
C_4H_4N-CN + H	–325	7	0.012	0.015	0.015	0.029
C_4NH_4CN + H	–295	9	0.011	0.011	0.011	0.011
cyclic-CHCHCHCHNCN + H	–174	2	0.093	0.183	0.198	0.229

Table 3. Theoretical channel-specific product BFs for the N(^{2}D) + C_5H_5N reaction at three temperatures (50 K, 200 K, and 300 K) and at E_c= 33.5 kJ/mol, starting from the i2-*i* intermediate.

Product channel	ΔH^0_0 (kJ/mol)	Channel number	T = 50 K	T = 200 K	T = 300 K	E_c=33.5 kJ/mol
C_4H_4N(pyrrolyl) + HCN	–426	1	0.583	0.577	0.567	0.538
1H-pyrazolyl + C_2H_2	–201	4	0.196	0.196	0.196	0.197
C_5H_5 (cyclopentadienyl) + N_2	–584	5	0.114	0.116	0.119	0.127
C_4NH_4CN + H	–302	8	0.025	0.025	0.025	0.026
Cyclic-CHCHCHCHCN$_2$ + H	–71	6	0.082	0.086	0.093	0.112

channel leading to the isomeric product (1H-pyrazolyl) and C_2H_2 (channel (4)) has comparable BFs (0.196 at 50 K and 0.197 under CMB conditions). The formation of one or more 7-membered ring products with different structures is always significant, with the largest yield associated with the formation of cyclic-CHCHCHCHNCN in channel (2) from i6 (0.093 at 50 K and 0.229 under CMB conditions). The channels (5) leading to cyclopentadienyl + N_2 is also significant when considering the i2-*i* PES portion. All the other product channels appear to contribute marginally to the global reactive flux, showing very small values of BFs. Overall, there is a mild dependence on the available energy for most channels. Nevertheless, the yields of the 7-membered ring products clearly increase with the total energy while the yield of the main channel (pyrrolyl + HCN) decreases. We were unable to estimate the possible contributions of the H-abstraction mechanisms, but we expect them to be minor by analogy with the $O(^1D) + C_6H_6$ reaction.

As already mentioned, there are no obvious ways to quantify how the reactive flux is distributed among the different initial intermediates because all pathways 1-6 were found to be barrierless (see Figure S1). Therefore, we decided to treat the system as statistical already in the first portion of the PES associated with the entrance channels. Given the absence of the *ortho* addition intermediate and the very reduced stability of intermediates i1 and i2 (which readily isomerize to i3 and i6 due to the very low transition states involved), we estimated the partitioning of the reactive flux by considering the DOS of the i3, i6 and i1-*i*/i2-*i* intermediates, *i.e.* the first intermediates along the pathways 1-6 that can have a significant lifetime. This is a rather rough approximation that, however, does not affect the BF of the most important channels while it has some effect on the minor ones.

For this reason, we propose the global BFs calculated in this way in Table 4, to be compared with the experimental data. We remind the reader that we do not distinguish 1H-pyrazolyl from 1H-imidazolyl or the possible H-displacement isomeric products experimentally.

The DOS values, that depend on the relative energy of the stationary points and on geometrical parameters (which affects the values of vibrational frequencies and rotational constants), are reported in Table S1 of the Supporting Information. In the evaluation of the relative importance of the partial BFs associated with i3, i6 and i1-*i*/i2-i we have multiplied by a factor of 2 those of i3, i6 and i2-*i* because of the possibility of a symmetrical bridge addition.

Overall, by inspecting both the partial and global values of the BFs, the title reaction is characterized by the competition between three main reaction channels: (*i*) ring-contraction

followed by formation of the pyrrolyl radical and HCN (common to all identified pathways), (*ii*) H loss, to form essentially a 7-membered ring co-product (whose structure is different for the different pathways) and (*iii*) ring-contraction followed by formation of 1H-imidazolyl/1H-pyrazolyl radical and acetylene.

Table 4. Experimental BFs at E_c= 33.5 kJ/mol (see Section 5.1) compared with the proposed global channel-specific product BFs derived by merging the theoretically predicted BFs starting from i3, i6 and i2-*i* intermediates (see text). The theoretical weighted global channel-specific product BFs obtained with the same methodology at 300 K and 200 K are also reported.

Product channels	Channel number	E_c=33.5 kJ/mol		T=300 K	T=200 K
		EXPT	THEORY		
pyrrolyl + HCN	1	0.61 ± 0.20	0.54	0.57	0.59
1H-pyrazolyl + C_2H_2	4	0.11 ± 0.06	0.11	0.11	0.11
1H-imidazolyl + C_2H_2	3		0.09	0.09	0.10
cyclopentadienyl + N_2	5		0.07	0.07	0.06
$C_5H_4N_2$ + H	7-10	0.28 ± 0.10	0.03	0.03	0.02
cyclic-CHCHCHCHNCN + H	2		0.07	0.06	0.05
cyclic-CHCHCHCHCN_2 + H	6		0.06	0.05	0.05
cyclic-CHCHNCHCHCN + H	11		0.03	0.02	0.02

5. IMPROVED ANALYSIS OF EXPERIMENTAL DATA AND COMPARISON WITH THEORETICAL PREDICTIONS

Our preliminary analysis of the experimental data reported in Ref. 49 indicated the occurrence of two main classes of product channels associated with (*i*) H-displacement or (*ii*) ring-contraction mechanisms with the formation of two heavy products. As already noted in Ref. 49, the experimental resolution did not permit us to disentangle the relative contributions of the various

possible isomeric $C_5H_4N_2$ co-products of the H-displacement channels or to assess the relative contributions of the heavier co-products of energetically possible HCN, C_2H_2, CN, and N_2 forming channels. Therefore, the preliminary best-fit was carried out using only two sets of $T(\theta)$ and $P(E'_T)$ functions, one referring to a global H-displacement channel (assuming that the most probable H-channels was the most exothermic one) and the other to the HCN forming channel (expected to be the main ring-contraction channel by analogy with the $N(^2D)$ + benzene reaction, as assessed in our recent publication[43]). Using this approach, we could not well reproduce the detailed shapes of product angular distributions simultaneously at both *m/z* = 65 and 66.[49] However, in the absence of theoretical support, a fit using more than two contributions was not warranted. At the time we anticipated that theoretical work on the full PES was planned.

After the PES and RRKM predictions of product BFs performed in the present work, we can now reconsider the preliminary fit of the data by exploiting the theoretical predictions to assist a more detailed interpretation of the experimental results. It is important to underline that the shapes of the CM product angular distributions derived in the preliminary fit of Ref. 49 are clearly indicating that the reaction proceeds via the formation of a long-lived complex,[79] thus justifying the use of an RRKM approach. The revision of the LAB data fit has the aim to verify whether the experimental data can be reproduced using the theoretical BFs or whether BFs somewhat different from the theoretical ones are actually required. This approach ultimately leads to the elucidation of the detailed reaction mechanism.

We recall that reactive scattering signals were observed[49] at:

(a) *m/z* = 92 ($C_5H_4N_2^+$), which is the mass of the parent ion of the molecular co-product in all the energetically open H-displacement channels (2, 6-11) (see Figures 2-4 of the PES);

(b) *m/z* = 91 ($C_5H_3N_2^+$), which is the (–1) daughter ion of the *m/z* = 92 product;

(c) *m/z* = 67 ($C_4H_5N^+$), which could be the mass of the parent ion of 1H-imidazolyl and 1H-pyrazolyl radicals possibly produced in channels (3) and (4), respectively, and/or of the pyrrole isomer produced in channel (12). Note that daughter ions of co-products associated to the H-displacement channels at this *m/z* are not expected, because it would require the emission of a C_2H moiety in the dissociative ionization process, an unlikely process;

(d) *m/z* = 66 ($C_4H_4N^+$), which is either the mass of the parent ion of the pyrrolyl radical (channel (1)) or the (–1) daughter ion of 1H-imidazolyl/1H-pyrazolyl and pyrrole from

channel (3), (4), and (12), respectively. Note that daughter ions from co-products associated to the H-displacement channels can also contribute to this *m/z* signal;

(e) *m/z* = 65 ($C_4H_3N^+$), which can be associated to daughter ions of the molecular/radical products of all channels mentioned above, including channel (5);

(f) *m/z* = 41, a likely daughter ion from heavy co-products of H-displacement channels, and perhaps from also ring-contraction channels.

The velocity vector (so called "Newton") diagram for the N(^{2}D) + pyridine experiment is depicted in Figure 6. In the figure the circles superimposed on the Newton diagram correspond to the maximum velocity that each indicated product can attain by assuming that all the total available energy E_{TOT} ($E_{TOT} = E_c - \Delta H_0^0$) is channeled into product translational energy. Only the four products predicted by RRKM to be most abundant (see Table 4) are shown. The circles related to the H-displacement channels have been represented with just one circle which refers to the statistically most favored H-forming channel (2) leading to cyclic-CHCHCHCHNCN (indicated as $C_5H_4N_2$ in Figure 6) formation; the corresponding circles for the heavy co-products of the other slightly less or more exothermic H- forming channels would have only slightly smaller or larger radius, respectively, and would barely be discernible on the scale of the figure. The Newton diagram reported here is different with respect to the one reported in Ref. 49, where the circle related to the H-displacement channels was drawn by considering the most exothermic H-forming channel (7) leading to 1H-pyrrole-1-carbonitrile ($C_5H_4N_2$), the circles associated with C_4H_4N (pyrrolyl) (+ HCN) and with C_4H_5N (3H-pyrrole) (+ CN) were shown, and the two circles associated with the C_2H_2 forming channels were missing.

Note that in the previous report[49] the relative intensities at *m/z* = 92, 67, 66, 65, and 41 were erroneously reported as 1.00, 0.08, 0.28 0.91, and 0.94. A careful revision has indicated that in the signal at *m/z* = 92 was included an incorrect intensity of also the daughter ion *m/z* = 91. In addition, the *m/z* = 67 small intensity was based only on a single measurement at the peak of the angular distribution and could not be verified whether all signal was clean reactive signal and, as such, it was not included in the estimate of the product BFs. Full angular distribution data were only recorded at *m/z* = 66 and 65, which correspond to the parent ion and the (–1) daughter ion of the pyrrolyl radical as well as from the (–1) daughter ion of the imidazolyl and pyrazolyl radicals but could also in part arise from daughter ions of the co-products of H-forming channels. Because the pyrrolyl component can be separated from that of the H-forming channels, we know the ratio

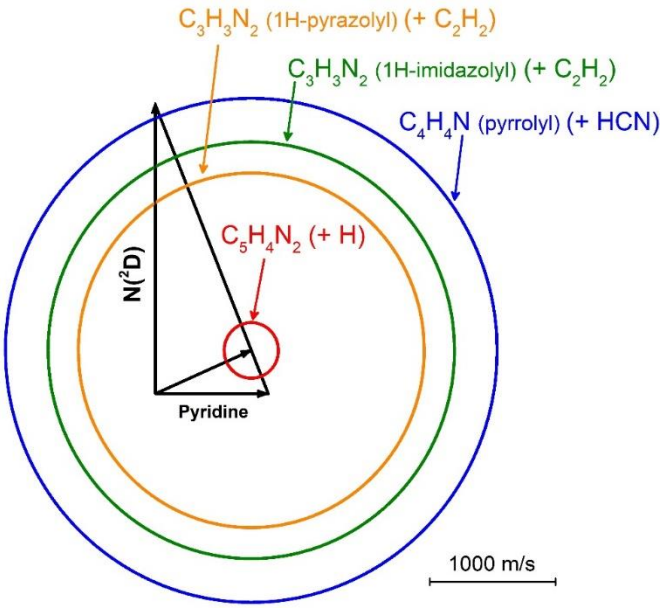

Figure 6. Velocity vector ("Newton") diagram for the $N(^2D)$ + pyridine reaction (E_c = 33.5 kJ/mol) where the concentric circles delimit the maximum velocity that the possible indicated primary products can attain in the CM system if all the available energy goes into product translational energy. The circles delimit also the LAB angular range within which the indicated primary products can be scattered. The four most relevant reactive channels are indicated: $C_5H_4N_2$ (+ H) (red circle), drawn by considering the energetic of channel (2) which has the largest RRKM BF among the H-displacement channels; the two isomeric $C_3H_3N_2$ (1H-imidazolyl and 1H-pyrazolyl) (+ C_2H_2) channels (3) (green circle) and (4) (orange circle), respectively; C_4H_4N (pyrrolyl) (+ HCN) channel (1) (blue circle).

(parent ion)/((–1) daughter ion) of pyrrolyl. In the revision we have assumed that at 17 eV the reactive signal at *m/z* = 67 could only be due to the parent ion of the imidazolyl/pyrazolyl, in a fraction (0.35) with respect to the (–1) daughter ion equal to that of pyrrolyl. After this correction, the most intense reactive signal is associated with *m/z* = 41. The revised relative intensities of the reactive signal at *m/z* = 92, 91, 67, 66, 65, and 41 (at 17 eV electron energy) are 0.73, 0.17, 0.003, 0.30, 0.97, and 1.00, respectively at Θ = 68° (which is close to the CM angle). Finally, as pyrrolyl does not give significant (-2) ion intensity at 17 eV, we have assumed the same for imidazolyl/pyrazolyl. These assumptions appear to be supported by the data analysis and theoretical predictions of BFs (see section 5.1 for the present overall revision of the product BFs). The relative amount of mass 67 contributing to the small, total reactive signal corresponding to imidazolyl/pyrazolyl products, is only 24% of the total, the main amount appearing at the (–1) daughter ion *m/z* = 66. Since the experimentally estimated BF of the C_2H_2 elimination channels

(which could include also the N_2 elimination channel) is 0.11 ± 0.06 (see Table 4), we think that the uncertainty associated to the *m/z* = 67 relative contribution is accounted for in the large error bars of more than 50% for the BF of these channels.

As discussed in Ref. 49, angular distributions were measured for only *m/z* = 92, 66, 65, and 41, because the signal-to-noise ratio at *m/z* = 91 and 67 was too low. The angular distribution at *m/z* = 92, 66, 65, and 41 are portrayed in the Figures 7(a), 7(b), 7(c), and 7(d), respectively. Note that the error bars at *m/z* = 41 are considerably larger than at *m/z* = 65, despite the similar reactive signals, because the background in the detector at *m/z* = 41 was substantially higher than at *m/z* = 65. In contrast, TOF distributions were only measured for *m/z* = 65, which yielded the best signal-to-noise (S/N) ratio and carries the fingerprints of both H-displacement and ring-contraction channels. The TOF distributions at *m/z* = 65 for three different LAB angles are shown in Figure 8.

The reported measurements at *m/z* = 92 were performed using 70 eV electron energy (count rate 30 counts/s), while for *m/z* = 66, 65, and 41 *soft* electron ionization at 17 eV was employed, because it permitted a significant reduction of interferences from fragmentation of higher mass species. For *m/z* = 92, a measurement at the CM angle using 17 eV electron energy (count rate 11 counts/s) was also acquired for normalization purposes. Count rate for *m/z* = 41 was 15 counts/s at 17 eV.

As can be seen from Figure 7(d), the *m/z* = 41 angular distribution is, within the error bars, similar to that measured at *m/z* = 92, indicating that it originates from dissociative ionization of the heavy co-product(s) of the H-displacement channel(s). In contrast, the LAB angular distributions measured at *m/z* = 66 and 65 (see Figures 7(b) and 7(c)), while exhibiting the central part (peaked around the CM angle) similar to the *m/z* = 92 distribution (see Figure 7(a)), exhibit a clear tail (or shoulder) extending significantly towards smaller angles (forward direction) (the backward direction could not be explored because measurements beyond 80° were not possible due to the closeness to the detector of the direction of the pyridine beam). This indicates that other reactive contributions are also present in the *m/z* = 66 and 65 angular distributions, arising from other channels besides those contributing to *m/z* = 92 and 41, and exhibiting very different kinematics and dynamics.

It should be noted (see Figures 7(b) and 7(c)) that the contribution of the tail (or shoulder) (at small angles) to the angular distributions, with respect to the main peak centered around the CM,

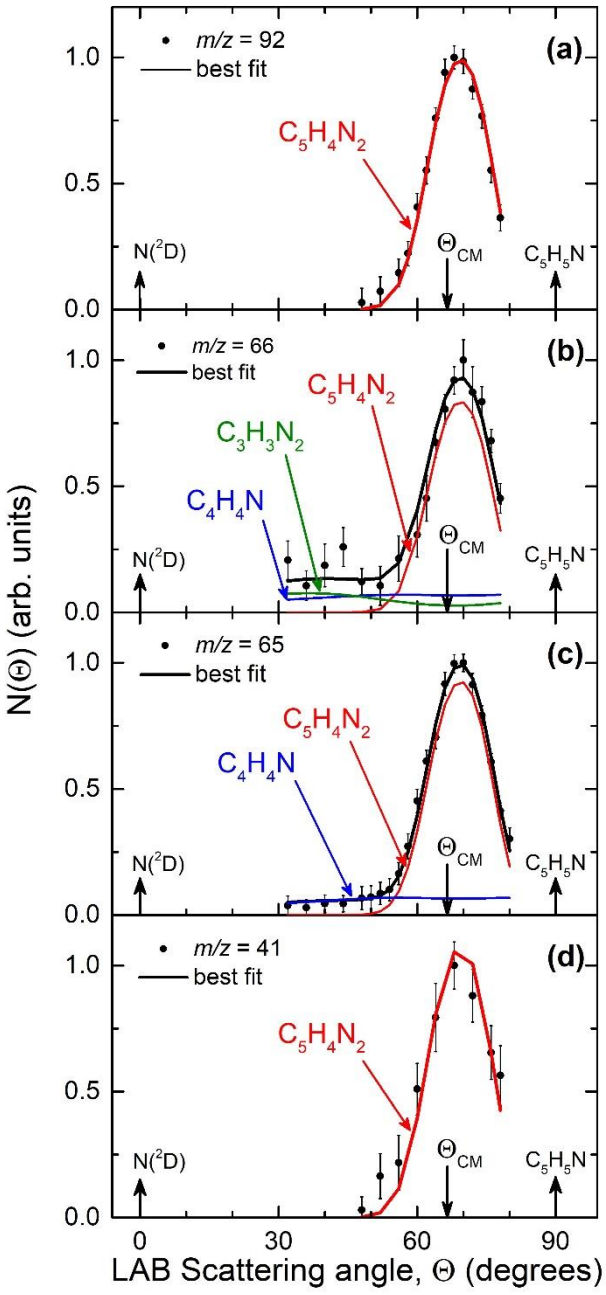

Figure 7. LAB angular distributions measured at *m/z* = 92, 66, 65 and 41 for the N(^{2}D) + pyridine reaction using soft ionization (17 eV). The solid lines (red in (a) and (d), and black in (b) and (c)), superimposed on the experimental data (black dots, with ±1σ error bars indicated) correspond to the calculated global best-fit by using the CM functions depicted in Figure 9. The separate contributions to the calculated global LAB angular distribution are color coded and indicated with the formula of the corresponding product (colors as in Figure 6: red (7-membered ring $C_5H_4N_2$), blue (pyrrolyl C_4H_4N), green (imidazolyl $C_3H_3N_2$).

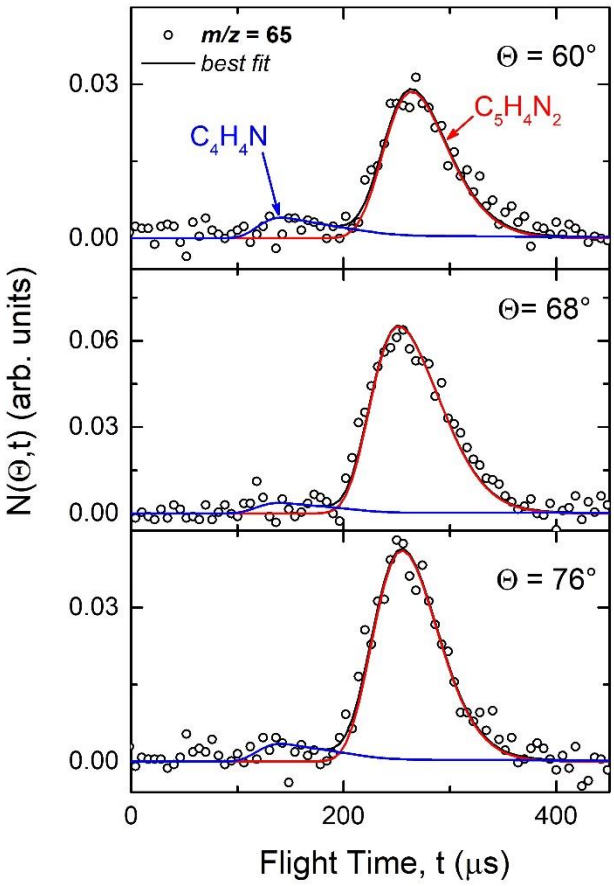

Figure 8. TOF distributions measured for *m/z* = 65 at LAB angles of 60°, 66° and 75° by applying soft ionization (17 eV). The reactive signal of the very fast small components is fit with the C_4H_4N (pyrrolyl) + HCN channel (blue line) while the slow dominant peak corresponds to the $C_5H_4N_2$ + H channel (red line).

is lower for *m/z* = 65 than for *m/z* = 66. Since we recorded only a weak signal at *m/z* = 67 (parent ion of pyrrole, and also of imidazolyl/pyrazolyl) and we know that pyrrole fragments little (about 7% at 300 K and 70 eV electron energy) to the (–1) daughter ion *m/z* = 66 and none to *m/z* = 65, the strong reactive signal at *m/z* = 65 cannot be attributed to a (–2) daughter ion of pyrrole, especially at 17 eV electron energy, but rather it reflects the (–1) daughter ion of the pyrrolyl radical (parent mass 66), which is instead expected to fragment substantially in the ionizer to *m/z* = 65, even at 17 eV. We remind that *m/z* = 67 also corresponds to the parent mass of imidazolyl/pyrazolyl, which are expected to fragment substantially to the (–1) daughter ion of 66 (similarly as pyrrolyl fragments substantially to the (–1) daughter ion). That is, we do not expect

imidazolyl/pyrazolyl to fragment significantly to *m/z* = 65. Therefore, we have indication that signals observed at *m/z* = 66 and 65 come mainly from the pyrrolyl radical (with HCN co-product) from channel (1)) rather than from the pyrrole (or isomer of it) (with CN co-product) from channel (12); but, notably, imidazolyl/pyrazolyl from channels (3)/(4) can also contribute somewhat to the *m/z* = 66 signal, as well as being responsible of a small reactive signal observed at the parent mass *m/z* = 67.

Since from the above arguments we have ruled out the occurrence of the CN forming channel (and this is corroborated by theory which finds it to have a negligible BF), and considering that theory predicts the N_2 forming channel to have a BF of only 0.07 and the pyrazolyl/imidazolyl forming channels of 0.11/0.09 (see Table 4), we have attempted a more refined best-fit of the experimental data than we did in the earlier Letter,[49] using in the simulations the statistically predicted BFs of the three main channels (H-displacement, HCN forming, and pyrazolyl/imidazolyl (theoretical global BF = 0.20) forming), to verify whether they are consistent with the experimental data. Therefore, the simultaneous best-fit of the product angular and TOF distributions at *m/z* = 66 and 65 was carried out using three different sets of $T(\theta)$ and $P(E'_T)$ functions, one set associated with the theoretically predicted predominant H forming channel (2) (BF = 0.07), and the other two sets to the pyrrolyl + HCN channel (1) (BF = 0.54) and 1H-imidazolyl/1H-pyrazolyl + C_2H_2 channels (3) and (4) (global BF = 0.20). These channels are theoretically the most sizeable product channels (see Table 4). Within this simulation the functions associated to channel (2) can also reflect other H-displacement channels which cannot be disentangled experimentally. That is, these $T(\theta)$ and $P(E'_T)$ functions are overall best-fit functions for H-displacement channels. Analogously, the functions associated to channel (3) (BF = 0.09) can also encompass channel (4) (pyrazolyl, BF = 0.011).

As can be seen from the Figures 7 and 8 the new, improved best-fit of the data is rather good. In particular, with respect to the original, simplified best-fit analysis of Ref. 49, it has been possible to account for the different relative contributions of the small angle shoulder in the angular distributions at *m/z* = 66 and 65. Specifically, this indicates that 1H-imidazolyl/1H-pyrazolyl (parent mass 67) fragments more to *m/z* = 66 than to *m/z* = 65 with respect to pyrrolyl (parent mass 66) that fragments strongly to *m/z* = 65). That is, 1H-imidazolyl/1H-pyrazolyl are mainly detected at *m/z* = 66 (the fraction at *m/z* = 67 is estimated using the previously estimated fragmentation of

pyrrolyl); in fact, the contribution of 1H-imidazolyl/1H-pyrazolyl is negligible in the simulation of the angular distribution at *m/z* = 65) (see Figure 7(c)).

The corresponding best-fit CM T(θ) and P(E'_T) functions for the three dominant channels (2), (1), and (3)/(4), used to simulate the data in the present, improved fit, are shown in Figure 9. It can be appreciated that also in the revised fit the T(θ)s of the three main channels are backward-forward symmetric (although with a somewhat different degree of polarization), and this indicates that the reaction proceeds via a long-lived complex mechanism[79] confirming that it can be treated with a statistical approach, as done here. The hatched areas in Figure 9 represent the CM functions that still afford an acceptable fit of the data.

The P(E'_T) distribution (Figure 9-*rhs*) for the H-displacement channel(s) peaks away from zero (at about 40 kJ/mol) with a tail extending up to slightly above 200 kJ/mol. In the figure, the total available energies ($\mathbf{E_{TOT}}$) for channels (2), (7), and (6) are indicated with arrows. Based on those characteristics we cannot exclude that also H-displacement channels other than (2) and (6) do contribute to the reactive signal, including the most exothermic channel (7), because the molecular product can be formed in highly excited internal states. The fraction of the total energy released as product translational energy, $\langle f_T \rangle$, relative to the maximum E'_T of the prominent channel (2), is 0.40. Since the P(E'_T), within its error bars, extends beyond the E_{TOT} for channel (2), a small fraction of also channel (7) is likely to contribute. Indeed, the P(E'_T) for the overall forming channels (Figure 9-*rhs*-top panel) is well consistent with predominant channels (2) and (6) and a minor channel (7). Note that theory predicts an overall BF of 0.19 for the H forming channels, with specifically BF = 0.07, 0.06, 0.03, and 0.03 for the channels (2), (6), (11) and (7-10), respectively (see Table 4). Note also that the contribution of channel (7) is calculated to be the largest one among the minor four H-channels (7-10) listed in the Tables 1-3, that give an overall BF = 0.03 (see Table 4). Overall, the experimental BF of 0.28 ± 0.10 agrees, within the error bars, with the theoretical BF of 0.19 for all the H-displacement channels.

The P(E'_T) of the HCN forming channel (1) dies off at the maximum total available energy of this channel, and $\langle f_T \rangle$ is 0.32, indicating that 68% of the total available energy goes into internal excitation of the pyrrolyl and HCN products (see Figure 9-*rhs*-middle panel). The data at *m/z* = 65 could also contain some contribution from the parent ion of cyclopentadienyl (+ N_2) (channel (5)); however, experimentally we are not sensitive to this contribution, which theoretically is predicted to be minor (BF of 0.07 vs 0.54) with respect to the dominant pyrrolyl (+ HCN) channel (1). Also

the P(E'$_T$) of the 1H-imidazolyl/1H-pyrazolyl + C_2H_2 channels (3) and (4) dies off at about E_{TOT} of the most exothermic of the two channels and reflects a <f_T> of 0.35 (for 1H-imidazolyl), which implies that about 65% of the total available energy goes into internal (ro-vibrational) excitation of the molecular/radical co-products.

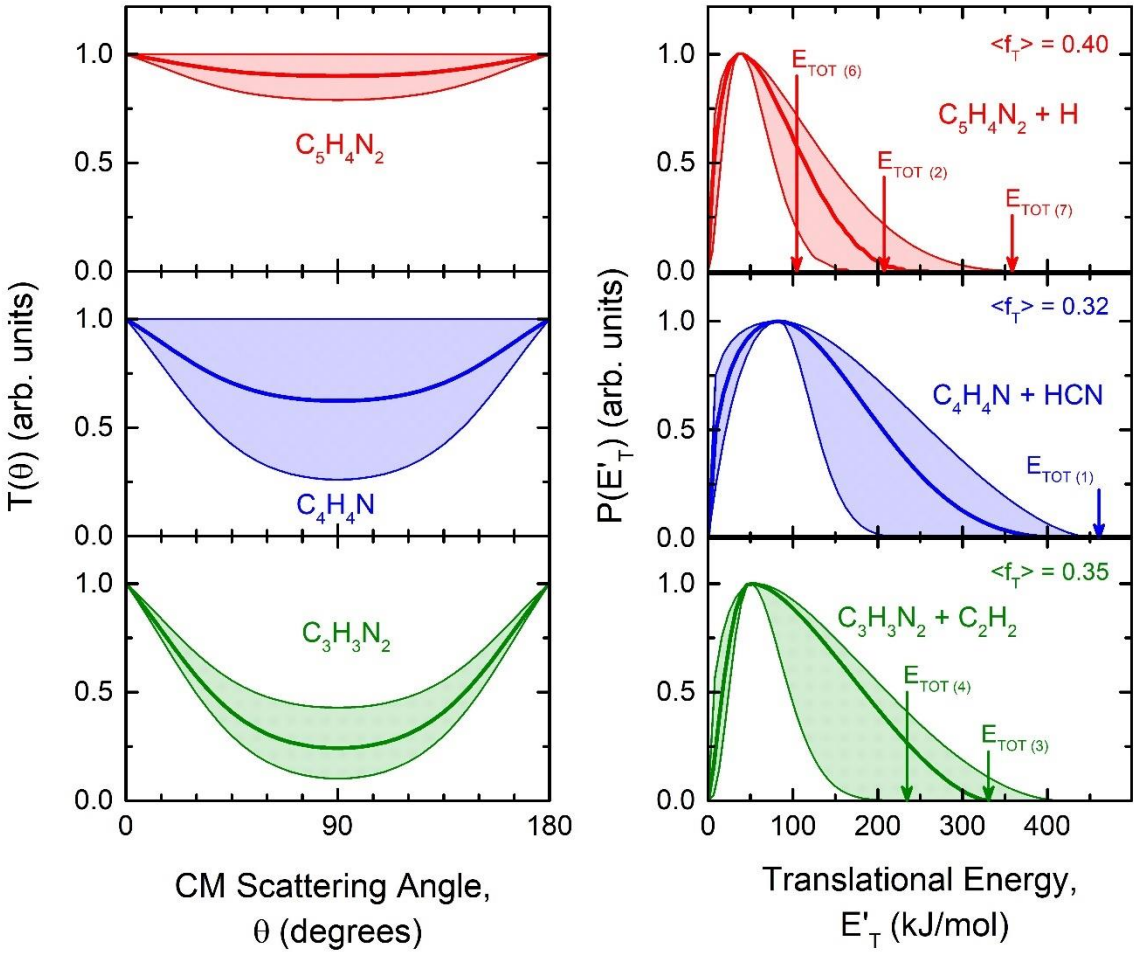

Figure 9. Best-fit CM angular distributions (left-hand-side) and best-fit CM translational energy distributions (right-hand-side) determined for the reactive channels of $C_5H_4N_2$ + H (red) and C_4H_4N + HCN (blue) from the reaction of N(^{2}D) + pyridine. The total energy (E_{TOT}) for each reactive channel is reported with the corresponding number of each channel indicated. While the translational energy fractions ($\langle f_T \rangle$) are reported those calculated with the most exothermic channel for each case. The shaded areas represent the error bars determined for the CM functions.

5.1. Product branching fractions. Experimental product BFs were derived following the procedure developed by Schmoltner et al.[80] and used by us extensively in recent years for a variety of multichannel reactions.[71,81] With respect to our previous Letter[49] we have revised the original

preliminary estimate of the product BFs taking in account, in addition to the improved 3-channels analysis described here, (*i*) the corrections of the relative intensity at *m/z* = 92, 91, and 67 described above and (*ii*) a different fragmentation pattern of the pyrrolyl and imidazolyl/pyrazolyl radicals to the (−1) daughter ion which is now assumed to be similar. At 17 eV the parent and the (−1) daughter ions are in the ratio 0.35/1.00, with an overall contribution at lower daughter ion fragments very small (*ca*. 0.11), as inferred from the dramatic reduction of the fragmentation of pyrrole (both at 300 K and 900 K, the latter mimicking an internally hot reaction product) when the ionizing electron energy is lowered from 70 eV to 17 eV.

The experimental BFs derived in the present analysis are given in Table 4. Experimentally we could achieve an improved best-fit of the data with three main sets of product channels: that corresponding to H-displacements, with overall BF = 0.28 ± 0.10, and those corresponding to two ring-contraction channels. Of the latter channels, one (dominant) is channel (1) leading to pyrrolyl + HCN (BF = 0.61 ± 0.20) while the other one leads to 1H-imidazolyl/1H-pyrazolyl + C_2H_2 (channels (3)/(4), BF = 0.11 ± 0.06). Remarkably, now the ratio of the BFs of the ring-contraction and H-displacement channels, (0.72±0.20)/(0.28±0.10) is reversed with respect to the value of (0.35±0.15)/(0.65±0.20) estimated in the previous report. The main reason of this difference comes, within the 3-channel analysis suggested by theory, from the estimate of the similar fragmentation pattern of the pyrrolyl and imidazolyl/pyrazolyl radical products. Note that the information from theory about the dominant relevance of the pyrrolyl channel (1) and the imidazolyl/pyrazolyl channels (3) and (4) has been crucial. The new product BFs are also much more in line with the experimental/theoretical study on the related N(^{2}D) + C_6H_6 reaction, for which the HCN formation was largely dominant. Those findings prompted the present theoretical work and the re-analysis of the CMB data of Ref. 49.

Experimentally, the ratio between the ring-contraction channels and the H-displacement channels is about 2.6±1.5, and this is somewhat lower than the value of about 4.3 predicted by theory. In fact, as can be seen in Table 4, according to the theoretical predictions, the dominant product channel at E_c = 33.5 kJ/mol is channel (1) leading to pyrrolyl + HCN (BF = 0.54). Among the possible ring-contraction channels, second in importance are channels (4)/(3) leading to (1H-pyrazolyl)/(1H-imidazolyl) + C_2H_2 (BF = 0.11 and 0.09, respectively), with formation of 1H-pyrazolyl + C_2H_2 (BF = 0.09) mainly occurring from the *i*-addition (see Table 3) (and only in very minor part (see Table 1) from other pathways). Notably, cyclopentadienyl + N_2 (channel (5)), only

formed from *ipso* addition (see Table 3), has a smaller BF of 0.07. The third most important channels are those leading to the 7-membered ring (cyclic-CHCHCHCHNCN) + H (channel (2) (BF = 0.07), with the other two isomeric 7-membered ring product channel (6) and (11) having BF = 0.06 and 0.03, respectively (see Table 4). Four other isomeric H-displacement channels being minor, with global BF = 0.03 for channels (7-10), among which channels (7) and (8) give the largest contribution (see Tables 2 and 3).

6. DISCUSSION

In discussing the present experimental/theoretical results on the N(^{2}D) + pyridine reaction it is useful to refer to the experimental/theoretical results recently published on the related N(^{2}D) + benzene reaction that we studied at the comparable collision energy of 31.8 kJ/mol.[43] The latter reaction was found to proceed via barrierless addition of N(^{2}D) to the aromatic ring of benzene, followed by the formation of several cyclic (five-, six-, and seven-membered ring) intermediates that undergo unimolecular decomposition to bimolecular products. The large value of the rate coefficient (*ca.* 2×10^{-10} cm^3 s^{-1} over the 50–296 K explored range) corroborated the theoretical prediction of a barrierless reaction.[43] At the E_c of 31.8 kJ/mol the ring-contraction channel was experimentally found to be largely dominant (BF = 0.92 ± 0.04), with a minor contribution (BF = 0.08 ± 0.04) coming from H-displacement channels. Theoretically, it was possible to disentangle the observed ring-contraction channel into two contributions: a dominant C_5H_5 + HCN product channel (BF = 0.745) and a minor C_4H_4N (pyrrolyl) + C_2H_2 product channel (BF = 0.056). At the same time, the H-displacement channels were theoretically predicted to be associated to the formation of *o*-C_6H_5N (*o*-N-cycloheptatriene radical) (BF = 0.135), C_5H_5CN (cyanocyclopentadiene) + H (BF = 0.053), and *p*-C_6H_5N (*p*-N-cycloheptatriene radical) + H (BF = 0.011). A mild dependence of the BFs on the temperature (or E_c) was noted, mostly affecting only the *o*-C_6H_5N + H vs the HCN channels relative yield.

After the data analysis revision presented here, the reaction mechanism of N(^{2}D) with the isoelectronic pyridine turns out to be quite similar to that with benzene as the ring contraction channel(s) are now dominant while the H-displacement channels are minor. However, the experimental BF for the H-displacement channels is substantially larger for N(^{2}D) + pyridine (by more than a factor of two) than for N(^{2}D) + benzene (BF = 0.28 ± 0.10 *vs* 0.08 ± 0.04). Also the

theoretical calculations point to some differences, with a smaller BF for the HCN channels (BF of 0.54 for pyridine *vs* 0.745 for benzene), a larger BF for the C_2H_2 channels (3) and (4) (global BF of 0.20 for pyridine *vs* 0.056 for benzene), and a similar BF for the H-displacement channels (global BF of 0.19 vs 0.199) (see Table 2 in Ref. 43 for N(^{2}D) + benzene BFs). The small yield of 1H-pyrrole-1-carbonitrile/2H-pyrrole-2-carbonitrile/3H-pyrrole-3-carbonitrile in channels (7-9) predicted for the N(^{2}D) + pyridine reaction has the equivalent (cyano-cyclopentadiene) in N(^{2}D) + benzene also formed with a small BF.[43] The very small yield of the 1H-ethynyl-1H-imidazole + H channel has its counterpart in very small yield of the channel leading to 1-ethynyl-1H-pyrrole + H in the reaction with benzene.

As for channels (1) and (12) (HCN + C_4H_4N and CN + C_4H_5N products, respectively), statistical calculations indicated that the situation is similar to that incurred in the related N(^{2}D) + benzene reaction,[43] where a dominant yield was predicted for the HCN channel and a negligible one for the CN channel. Clearly, similarities as well as differences are present when comparing the two systems.

We note that formation of $C_4H_4N_2$ (pyrimidine) + CH, a weakly exothermic channel (ΔH^0_0 = –59 kJ/mol) (not listed) could not be experimentally probed because its parent mass (*m/z* = 80) would be fully masked by the intense elastic peak of the very intense pyridine beam (mass 79) due to the ^{13}C natural isotope abundance. However, it was predicted to have a negligible BF in our RRKM calculations. Similar results were found in the reaction N(^{2}D) + benzene for the analogous channel leading to pyridine + CH (a similarly weakly exoergic channel) that was predicted by statistical RRKM calculations to be negligible with respect to H displacement and ring contraction channels.[43,82,83]

The present results have some implications both on the chemistry of the atmosphere of Titan as well as on N-doping of graphene in plasmas. Concerning the chemistry of Titan, our results contribute to clarifying the chemistry involving N-aromatic species. As already noted in the Introduction, pyridine has been searched for in the atmosphere of Titan but a dedicated ALMA campaign could only derive an upper limit ∼1.15 ppb above 300 km assuming a constant profile. According to current photochemical models, the mole fraction of N(^{2}D) becomes significant above an altitude of 800 km[78,84] and a signal at *m/z*=80 (possibly protonated pyridine or one of its isomers) was recorded by INMS onboard Cassini between 1027 and 1200 km.[13] There are possible formation routes of pyridine including ion-molecule reactions[9] or the neutral-neutral reactions CH

+ pyrrole,[85] CN + 1,3-butadiene[16-19] and N(^{2}D) + benzene.[43,82,83] Our results indicate that, even if formed, pyridine can quickly undergo a chemical reaction with N(^{2}D) itself causing mostly ring-contraction processes, either with formation of the pyrrolyl radical + HCN or with formation of 1H-imidazolyl/1H-pyrazolyl + C_2H_2 and (to a lesser extent) of N_2 + cyclopentadienyl radical. The H-displacement channels are mainly represented by the formation of 7-membered ring radicals and, to a minor amount, of 1H-pyrrole-1-carbonitrile/2H-pyrrole-2-carbonitrile/3H-pyrrole-3-carbonitrile in channels (7-9). If formed, the possible fate of these species in the conditions of Titan will be to further react with the most abundant molecules and radicals at that altitude. In particular, as already noted in the case of the *o*-C_6H_5N radical formed in the N(^{2}D) + benzene reaction,[43] their reactions with atomic hydrogen (which is present in the thermosphere of Titan) will convert the 7-membered ring radicals formed in channels (2), (6) and (11) into pyrrolyl radical + HCN or 1H-imidazolyl/1H-pyrazolyl + C_2H_2, as can be clearly appreciated from the PES of Figures 2-4, once the 7-membered ring radicals and H act as reactants. 1H-pyrrole-1-carbonitrile/2H-pyrrole-2-carbonitrile/3H-pyrrole-3-carbonitrile and 1-ethynyl-1H-imidazole, instead, are closed-shell species that could accumulate under the conditions of Titan. Regarding the fate of the pyrrolyl radical, we note that, according to our CMB results on its formation channel, only 32% of the available energy goes into product translational energy, leaving 68% of it as internal energy of the two products. That means that the pyrrolyl radical can be formed with enough internal energy to decompose into C_2H_2 + CH_2CN, a process that needs +245.3 kJ/mol to overcome the highest transition state along the pyrrolyl decomposing pathway.[86] In conclusion, under the conditions of Titan, the title reaction will either lead to the formation of small aromatic or highly unsaturated N-rich cyclic compounds (thus contributing to the building-up of those complex structures that are called into play to either explain the IR emission band at 3.28 μm or the CAPS-IBS mass spectrum[11-13]) or to a significant degradation of pyridine toward much smaller and abundant moieties like HCN, C_2H_2, CH_2CN. Furthermore, the title reaction can be considered an efficient destruction route of pyridine that adds to the other possible reactions with charged species[18] and cannot be considered a formation route of pyrimidine.

Concerning the implication for the N-doping of graphene via the use of plasmas, we note here that the results we have obtained on this system as well on the related N(^{2}D) + benzene reaction can contribute to clarify the mechanism at play. It has been shown that the longer the exposure to the nitrogen plasma, the larger the number of nitrogen atoms that enter into the structure of

graphene will be. This is fully consistent with the results we have seen here as no reduction of reactivity is expected for the title reaction (in which the aromatic ring already contains nitrogen) with respect to the case of benzene since both are barrierless reactions. Also, the global reaction mechanisms are very similar and the only contribution that reduces the N-content of the molecular structure, that is the channel leading to N_2 + C_5H_5, was seen to be minor, even though it is the most exothermic channel of the title reaction. The analysis of the structure of N-doped graphite indicates the presence of 7-membered and 5-membered rings upon nitrogenation. This is also consistent with the structures that we have identified along the PES. Obviously, in the case of the N(^{2}D) reaction with graphene, most of the degrees of freedom which are typical of a gas phase reaction will be lost and the structures which are similar to those of the intermediates shown in Figures 2-4 are expected to be stabilized.

7. CONCLUSIONS

The PES of the reaction N(^{2}D) + C_5H_5N was calculated theoretically and the product BFs were derived from RRKM/ME statistical computations. The electronic structure calculations of the PES indicate that the reaction proceeds by barrierless addition of N(^{2}D) to pyridine. Some assumptions of how to partition the initial reactive flux were necessary. A revised analysis of previous CMB experimental data gave product BFs that are in line with the present theoretical predictions. Two main types of mechanisms are ruling the overall reaction: H-displacement and ring-contraction. The ring-contraction mechanisms leading to pyrrolyl + hydrogen cyanide and to 1H-imidazolyl/pyrazolyl + acetylene (and possibly also to some cyclopentadienyl + N_2) were found to be dominant in the CMB experiments (with BF of 0.61 ± 0.20 and 0.11 ± 0.06, respectively), in good agreement with RRKM predictions according to which the channel leading to pyrrolyl + HCN (BF = 0.54) and to 1H-pyrazolyl + C_2H_2 (BF = 0.11) and 1H-imidazolyl + C_2H_2 (BF = 0.09) dominate. H-displacement channels give a significant contribution in the CMB experiments (BF = 0.28 ± 0.10) as well as in the RRKM estimates (overall BF = 0.19), corresponding to the following channels: cyclic-CHCHCHCHNCN + H (channel (2)) (BF = 0.07), cyclic-CHCHCHCHCN$_2$ + H (channel (6) (BF = 0.06), cyclic-CHCHNCHCHCN + H (channel (11) (BF = 0.03), and several isomeric $C_5H_4N_2$ + H channels (overall BF = 0.03).

Pyrimidine is not formed through an N/CH exchange channel.

It is quite interesting that the main products of the title reaction are the pyrrolyl and imidazolyl/pyrazolyl radicals. These radical intermediates play key roles in atmospheric chemistry, combustion, biochemistry, and many other chemical processes due to their high reactivity. Numerous photochemistry experiments have been carried out on pyrrolyl and imidazolyl radicals and, very recently,[87] also direct spectroscopic measurements (using high-resolution photoelectron imaging and photodetachment spectroscopy of cryogenically cooled pyrrolide and imidazolide anions) have been reported to probe the electronic structure and spectroscopy of these important radicals.

The effect of increasing the energy available to the system is modest. Some competition between the ring-contraction channels (mainly pyrrolyl + HCN) and the H-displacement channels leading to 7-membered-ring molecules + H can be appreciated and rationalized by considering that a larger internal energy content will favor the prompt dissociation of the 7-membered intermediates against their isomerization. Under the conditions relevant for Titan thermosphere (T = 200 K), the yield of pyrrolyl (C_4H_4N) increases while that of the main 7-membered ring channels decreases with respect to the CMB conditions. The BF of the other very minor channels are not so sensitive to temperature. This information may be useful for theoretical modeling of the atmosphere of Titan.

A more general conclusion is that aromatic rings are not so resistant to the chemical attack as commonly believed, at least not in the case of very energetic reactants like electronically excited species. This is the fifth case we have investigated where ring-contraction of small aromatics (benzene or pyridine) is a significant (if not the dominant) reaction pathway, after O(^{3}P,^{1}D) + benzene (significant in the case of the ^{3}P reaction, dominant in the case of the ^{1}D reaction),[88,89] O(^{3}P,^{1}D) + pyridine (largely dominant in both cases),[23] O(^{3}P,^{1}D) + toluene (significant in the case of the ^{3}P reaction, dominant in the case of the ^{1}D reaction)[90] and N(^{2}D) + benzene (largely dominant).[43] It will be interesting to verify whether a similar mechanism is present also in the case of polycyclic aromatic hydrocarbons, such as naphthalene, which are supposed to accumulate in various environments because of their chemical stability.

A comment on the possible implications for prebiotic chemistry is in order. Our results indicate that the title reaction is an efficient destruction route of pyridine, provided that N atoms in the first electronically excited state can be produced by the photolysis of molecular nitrogen or other mechanisms. Such processes are active in the atmosphere of Titan and might have been possible

in the unshielded primitive terrestrial atmosphere. Contrary to what was previously suggested, not only is the N(^{2}D) + pyridine reaction not a viable way to produce pyrimidine, but it rather helps prevent pyridine buildup. It would have been very interesting to find a mechanism for the formation of the pyrimidine which is the backbone ring structure of several key biological molecules, that is, the nucleobases uracil (in RNA), cytosine (in RNA and DNA), and thymine (in DNA). Other formation routes will need to be explored.

Finally, the present results as well as those on the N(^{2}D) + C_6H_6 reaction help in understanding the mechanism of N-doping graphene via the use of plasma.

ASSOCIATED CONTENT

Supporting Information. Additional information is provided in Supporting information (see list below). This material is available free of charge at http://pubs.acs.org.

Figure S1: Plots of the scan calculations performed for the entrance channel considering all the six possible attacks for the N(^{2}D) + C_5H_5N reaction.

Figure S2: Schematic representation of the isomerization pathways originated form the i1, i2, i3 and i6 intermediates, identified in the potential energy surface for the N(^{2}D) + C_5H_5N reaction.

Figure S3: Schematic representation of additional isomerization pathways originated form the i1 and i2 intermediates, identified in the potential energy surface for the N(^{2}D) + C_5H_5N reaction.

Figures S4 and S5: Schematic representation of the potential energy surface for the N(^{2}D) + C_5H_5N reaction, obtained considering additional (less favorable) reaction pathways with respect to those reported in Figures 2-4 of the main text.

Table S1: Structures (in the form of cartesian coordinates) of the stationary points identified in the potential energy surfaces for the N(^{2}D) + pyridine reaction.

Table S2: RRKM unimolecular rate constants (in s^{-1}) for the relevant unimolecular processes reported in the potential energy surfaces in Figures 2-4.

Table S3: Density of states (DOS) calculated for the initial intermediates of the N(^{2}D) + pyridine reaction at the collision energy (E_c = 33.5 kJ/mol) and at two different temperatures (T = 300 K and T = 200 K).

AUTHOR INFORMATION

Corresponding Authors

Piergiorgio Casavecchia; orcid.org/0000-0003-1934-7891;
Email: piergiorgio.casavecchia@unipg.it
Nadia Balucani; orcid.org/0000-0001-5121-5683; Email: nadia.balucani@unipg.it

Notes

The authors declare no competing financial interests.

ACKNOWLEDGMENTS

This work was supported by the Italian Space Agency (Bando ASI Prot. n. DC-DSR-UVS-2022-231, Grant no. 2023-10-U.0 "Modeling Chemical Complexity: all'Origine di questa e di altre Vite per una visione aggiornata delle missioni spaziali (MIGLIORA)" Codice Unico di Progetto (CUP) F83C23000800005). This work has also been funded by the European Union - NextGenerationEU under the Italian Ministry of University and Research (MUR) National Innovation Ecosystem grant ECS00000041 – VITALITY. CUP: B43C22000470005.

REFERENCES

(1) Scriven, E. F. V.; Murugan, R. Pyridine and pyridine derivatives. *Kirk-Othmer Encyclopedia of Chemical Technology* (**2006**). https://doi.org/10.1002/0471238961.1625180919031809.a01.pub2

(2) Callahan, M. P.; Smith, K. E.; Cleaves, H. J.; Ruzicka, J.; Stern, J. C.; Glavin, D. P.; House, C. H.; Dworkin, J. P. Carbonaceous meteorites contain a wide range of extraterrestrial nucleobases. *Proc. Natl. Acad. Sci.* **2011**, *108*, 13995-13998.

(3) Smith, K. E.; Callahan, M. P.; Gerakines, P. A.; Dworkin, J. P.; House, C. H. Investigation of pyridine carboxylic acids in CM2 carbonaceous chondrites: Potential precursor molecules for ancient coenzymes. *Geochimica et Cosmochimica Acta* **2014**, *136*, 1-12.

(4) Pizzarello, S.; Huang, Y.; Becker, L.; Poreda,R. J.; Nieman, R. A.; Cooper, G.; Williams, M. The organic content of the Tagish Lake meteorite. *Science* **2001**, *293*, 2236-2239.

(5) Smith, K. E.; Gerakines, P. A.; Callahan, M. P. Metabolic precursors in astrophysical ice analogs: implications for meteorites and comets. *Chem. Comm.* **2015**, *51*, 11787-11790.

(6) Yasuhiro, O.; Koga, T.; Takano, Y.; Ogawa, N. O.; Ohkouchi, N.; Sasaki, K.; Sato, H.; *et al.* Uracil in the carbonaceous asteroid (162173) Ryugu. *Nature Comm.* **2023**, *14*, 1292.

(7) Friedmann, N.; Miller, S. L.; Sanchez, R. A. Primitive Earth synthesis of nicotinic acid derivatives. *Science* **1971**, *171*, 1026-1027.

(8) Nixon, C. A. The composition and chemistry of Titan's atmosphere. *ACS Earth and Space Chem.* **2024**, *8*, 406-456.

(9) Vuitton, V.; Yelle, R. V.; McEwan, M. J. Ion chemistry and N-containing molecules in Titan's upper atmosphere. *Icarus* **2007**, *191*, 722– 742.

(10) Nixon, C. A.; Thelen, A. E.; Cordiner, M. A.; Kisiel, Z.; Charnley, S. B.; Molter, E. M.; Serigano, J.; Irwin, P. G. J.; Teanby, N. A.; Kuan, Y.-J. Detection of Cyclopropenylidene on Titan with ALMA. *Astron. J.* 2020, 160, 205 (17 pp).

(11) López-Puertas, M.; Dinelli, B. M.; Adriani, A.; Funke, B.; García-Comas, M.; Moriconi, M. L.; D'Aversa, E.; Boersma, C.; Allamandola, L. J. Large Abundances of Polycyclic Aromatic hydrocarbons in Titan's upper atmosphere. *Astrophys. J.* **2013**, *770*, 132 (8 pp).

(12) Dinelli, B. M.; López-Puertas, M.; Adriani, A.; Moriconi, M. L.; Funke, B.; García-Comas, M.; D'Aversa, E. An unidentified emission in Titan's upper atmosphere. *Geophys. Res. Lett.* **2013**, *40*, 1489–1493.

(13) Haythornthwaite, R. P.; Coates, A. J.; Jones, G. H.; Wellbrock, A.; Waite, J. H.; Vuitton, V.; Lavvas, P. Heavy Positive Ion Groups in Titan's Ionosphere from Cassini Plasma Spectrometer IBS Observations. *Planet. Sci. J.* **2021**, *2*, 26.

(14) Herbig, G. H. The Diffuse Interstellar Bands. *Annu. Rev. Astron. Astrophys.* **1995**, *33*, 19– 73.

(15) Charnley, S. B.; Kuan, Y.-J.; Huang, H.-C.; Botta, O.; Butner, H. M.; Cox, N.; Despois, D.; Ehrenfreund, P.; Kisiel, Z.; Lee, Y.-Y. Astronomical searches for nitrogen heterocycles. *Adv. Space Res.* **2005**, 36, 137– 145.

(16) Morales, S. B.; Bennett, C. J.; Le Picard, S. D.; Canosa, A.; Sims, I. R.; Sun, B. J.; Chen, P. H.; Chang, A. H. H.; Kislov, V. V.; Mebel, A. M.; *et al.* A crossed molecular beam, low-temperature kinetics, and theoretical investigation of the reaction of the cyano radical (CN) with 1,3-butadiene (C_4H_6). A route to complex nitrogen-bearing molecules in low-temperature extraterrestrial environments. *Astrophys. J.* **2011**, *742*, 26 (10pp).

(17) Sun, B. J.; Huang, C. H.; Chen, S. Y.; Chen, S. H.; Kaiser, R. I.; Chang, A. H. H. Theoretical study on reaction mechanism of ground-state cyano radical with 1,3-butadiene: prospect of pyridine formation. J. *Phys. Chem. A* **2014**, *118*, 7715-7724.

(18) Parker, D. S. N.; Kaiser, R. I.; Kostko, O.; Troy, T. P.; Ahmed, M.; Sun, B.-J.; Chen, S.-H.; Chang, A. H. H. On the formation of pyridine in the interstellar medium. *Phys. Chem. Chem. Phys.* **2015**, *17*, 32000-32008.

(19) Parker, D. S. N.; Kaiser, R. I. On the formation of nitrogen-substituted polycyclic aromatic hydrocarbons (NPAHs) in circumstellar and interstellar environments. *Chem. Soc. Rev.* **2017**, *46*, 452-463.

(20) Bouwman, J.; Bodi, A.; Hemberger, P. Nitrogen matters: the difference between PANH and PAH formation. *Phys. Chem. Chem. Phys.* **2018**, *20*, 29910-29917.

(21) Satchin, S.; Taatjes, C. A.; Osborn, D. L.; Selby, T. M.; Trevitt, A. J.; Wilson, K. R.; Leone, S. R. Direct detection of pyridine formation by the reaction of CH (CD) with pyrrole: a ring expansion reaction. *Phys. Chem. Chem. Phys.* **2010**, *31*, 8750-8758.

(22) Peeters, Z.; Botta, O.; Charnley, S.B.; Kisiel, Z.; Kuan, Y.J.; Ehrenfreund, P. Formation and photostability of N-heterocycles in space-I. The effect of nitrogen on the photostability of small aromatic molecules. *Astron. Astrophys.* **2005**, *433*, 583-590.

(23) Recio, P.; Alessandrini, S.; Vanuzzo, G.; Pannacci, G.; Baggioli, B.; Marchione, D.; Caracciolo, A.; Murray, V . J.; Casavecchia. P.; Balucani, N.; *et al.* Intersystem crossing in the entrance channel of the reaction of O(^{3}P) with pyridine. *Nat. Chem.* **2022**, *14*, 1405-1412.

(24) Balucani, N.; Skouteris, D. Gas-phase prebiotic chemistry driven by ultraviolet photolysis of simple molecules. in *Prebiotic Photochemistry: From Urey–Miller-like Experiments to Recent Findings*, eds. Saija, F.; Cassone, J. The Royal Society of Chemistry, **2021**, 37-59.

(25) Ralchenko, Y.; Kramida, A E.; Reader, J. *NIST Atomic Spectra Database* (ver. 4.0.1), National Institute of Standards and Technology, Gaithersburg, MD, **2006**.

(26) Gelfand, N.; Komarova, K.; Remacle, F.; Levine, R. D. Nonadiabatic quantum dynamics explores non-monotonic photodissociation branching of N_2 into the N(^{4}S) + N(^{2}D) and N(^{4}S) + N(^{2}P) product channels. *Phys. Chem. Chem. Phys.* **2024**, *26*, 3274-3284.

(27) Balucani, N. *Chem. Soc. Rev.* **2012**, *41*, 5473–5483.

(28) Dutuit, O.; Carrasco, N.; Thissen, R.; Vuitton, V.; Alcaraz, C.; Pernot, P.; Balucani, N.; Casavecchia, P.; Canosa, A.; Picard, S. L.; *et al.* Critical review of N, N^+, N_2^+, N^{++}, and N_2^{++} main production processes and reactions of relevance to Titan's atmosphere. *Astrophys. J. Suppl. Ser.* **2013**, *204*, 20 (45 pp).

(29) Balucani, N.; Bergeat, A.; Cartechini, L.; Volpi, G. G.; Casavecchia, P.; Skouteris, D.; Rosi, M. Combined crossed molecular beam and theoretical studies of the N(^{2}D) + CH_4 reaction and implications for atmospheric models of Titan. *J. Phys. Chem. A* **2009**, *113*, 11138– 11152.

(30) Balucani, N.; Leonori, F.; Petrucci, R.; Stazi, M.; Skouteris, D.; Rosi, M.; Casavecchia, P. Formation of nitriles and imines in the atmosphere of Titan: combined crossed-beam and theoretical studies on the reaction dynamics of excited nitrogen atoms N(^{2}D) with ethane. *Faraday Discuss.* **2010**, *147*, 189– 216.

(31) Balucani, N.; Alagia, M.; Cartechini, L.; Casavecchia, P.; Volpi, G. G.; Sato, K.; Takayanagi, T.; Kurosaki, Y. Cyanomethylene formation from the reaction of excited nitrogen atoms with acetylene: a crossed beam and ab initio study. *J. Am. Chem. Soc.* **2000**, *122*, 4443– 4450.

(32) Balucani, N.; Cartechini, L.; Alagia, M.; Casavecchia, P.; Volpi, G. G. Observation of nitrogen-bearing organic molecules from reactions of nitrogen atoms with hydrocarbons: A crossed beams study of N(^{2}D) + ethylene. *J. Phys. Chem. A* **2000**, *104*, 5655– 5659.

(33) Balucani, N.; Skouteris, D.; Leonori, F.; Petrucci, R.; Hamberg, M.; Geppert, W. D.; Casavecchia, P.; Rosi, M. Combined crossed beam and theoretical studies of the N(^{2}D) + C_2H_4 reaction and implications for atmospheric models of Titan. *J. Phys. Chem. A* **2012**, *116*, 10467–10479.

(34) Vanuzzo, G.; Mancini, L.; Pannacci, G.; Liang, P.; Marchione, D.; Recio, P.; Tan, Y.; Rosi, M.; Skouteris, D.; Casavecchia, P.; Balucani, N.; Hickson, K.M.; Loison, J-C.; Dobrijevic, M. Reaction N(^{2}D) + CH_2CCH_2 (Allene): An experimental and theoretical investigation and implications for the photochemical models of Titan. *ACS Earth Space Chem.* **2022**, *6*, 2305-2321.

(35) Mancini, L.; Vanuzzo, G.; Marchione, D.; Pannacci, G.; Liang, P.; Recio, P.; Rosi, M.; Skouteris, D.; Casavecchia, P.; Balucani, N. The Reaction N(^{2}D) + CH_3CCH (Methylacetylene): A combined crossed molecular beams and theoretical investigation and implications for the atmosphere of Titan. *J. Phys. Chem. A* **2021**, *125*, 8846– 8859.

(36) Vanuzzo, G.; Marchione, D.; Mancini, L.; Liang, P.; Pannacci, G.; Recio, P.; Tan, Y.; Rosi, M.; Skouteris, D.; Casavecchia, P.; Balucani, N. The N(^{2}D) + CH_2CHCN (vinyl cyanide) reaction: A combined crossed molecular beam and theoretical study and implications for the atmosphere of Titan. *J. Phys. Chem. A.* **2022**, 126, 6110-6123.

(37) Liang, P.; Mancini, L.; Marchione, D.; Vanuzzo, G.; Ferlin, F.; Recio, P.; Tan, Y.; Pannacci, G.; Vaccaro, L.; Rosi, M. Combined crossed molecular beams and computational study on the N(^{2}D) + HCCCN($X^1\sum^+$) reaction and implications for extra-terrestrial environments. *Mol. Phys.* **2022**, *120* (1-2), e1948126.

(38) Mancini, L.; Rosi, M.; Skouteris, D.; Vanuzzo, G.; Pannacci, G.; Casavecchia, P.; Balucani, N. A computational characterization of the reaction mechanisms for the reactions N(^{2}D) + CH_3CN and HC_3N and implications for the nitrogen-rich organic chemistry of Titan. *Comp. Theor. Chem.* **2023**, *1229*, 114341

(39) Homayoon, Z.; Bowman, J. M.; Balucani, N.; Casavecchia, P. Quasiclassical trajectory calculations of the N(^{2}D) + H_2O reaction: Elucidating the formation mechanism of HNO and HON seen in molecular beam experiments. *J. Phys. Chem. Lett.* **2014**, *5*, 3508– 3513.

(40) Balucani, N.; Cartechini, L.; Casavecchia, P.; Homayoon, Z.; Bowman, J. M. A combined crossed molecular beam and quasiclassical trajectory study of the Titan-relevant N(^{2}D) + D_2O reaction. *Mol. Phys.* **2015**, *113*, 2296– 2301.

(41) Balucani, N.; Casavecchia, P.; Banares, L.; Aoiz, F. J.; Gonzalez-Lezana, T.; Honvault, P.; Launay, J. M. Experimental and theoretical differential cross sections for the N (^{2}D) + H_2 reaction. *J. Phys. Chem. A* **2006**, *110*, 817-829.

(42) Balucani, N.; Alagia, M.; Cartechini, L.; Casavecchia, P.; Volpi, G. G.; Pederson, L. A.; Schatz, G. C. Dynamics of the N(^{2}D)+D_2 Reaction from crossed-beam and quasiclassical trajectory studies. *J. Phys. Chem. A* **2001**, *105*, 2414– 2422.

(43) Balucani, N., Caracciolo, A., Vanuzzo, G., Skouteris, D., Rosi, M., Pacifici, L., Casavecchia, P.; Hickson, K.M.; Loison, J-C.; Dobrijevic, M. An experimental and theoretical investigation of the N(^{2}D) + C_6H_6 (benzene) reaction with implications for the photochemical models of Titan. *Faraday Discuss.* **2023** *245*, 327-351.

(44) Wang, H.; Maiyalagan, T.; Wang, X. Review on recent progress in nitrogen-doped graphene: synthesis, characterization, and its potential applications. *ACS Catalysis* **2012**, *2*, 781-794.

(45) Liang, H.; Ming, F.; Alshareef, H. N. Applications of Plasma in Energy Conversion and Storage Materials. *Adv. Energy Mater*. **2018**, *8*, 1801804.

(46) Wang, Y.; Shao, Y.; Matson, D. W.; Li, J.; Lin, Y. Nitrogen-doped graphene and its application in electrochemical biosensing. *ACS Nano* **2010**, *4*, 1790-1798.

(47) Begley, A.; Bartolomeo, G. L.; Abbott, D. F.; Mougel, V.; Zenobi, R. Nitrogen-doping graphene at ambient conditions with N2-DBD-plasma and the role of neutral species. *Plasma. Process. Polym.* **2023**, e2300168.

(48) Begley, A. I.; Shuman, N. S.; Long, B. A.; Ksmpf, R.; Gyr, L.; Viggiano, A. A.; Zenobi, R. Excited-state N atoms transform aromatic hydrocarbons into N-heterocycles in low-temperature plasmas. *J. Phys. Chem. A* **2022**, *126*, 1743–1754.

(49) Recio, P.; Marchione, D.; Caracciolo, A.; Murray, V. J.; Mancini, L.; Rosi, M.; Casavecchia, P.; Balucani, N. A crossed molecular beam investigation of the N(^{2}D) + pyridine reaction and implications for prebiotic chemistry. *Chem. Phys. Lett.* **2021**, *779*, 138852.

(50) Marchione, D.; Mancini, L.; Liang, P.; Vanuzzo, G.; Pirani, F.; Skouteris, D.; Rosi, M.; Casavecchia, P.; Balucani, N. Unsaturated dinitriles formation routes in extraterrestrial environments: A combined experimental and theoretical investigation of the reaction between cyano radicals and cyanoethene (C_2H_3CN). *J. Phys. Chem. A*. **2022**, *126*, 3569-3582.

(51) Mancini, L.; Rosi, M.; Skouteris, D.; Vanuzzo, G.; Pannacci, G.; Casavecchia, P.; Balucani, N. A computational characterization of the reaction mechanisms for the reactions N(^{2}D) + CH_3CN and HC_3N and implications for the nitrogen-rich organic chemistry of Titan. *Comp. Theor. Chem.* **2023**, *1229*, 114341.

(52) Pannacci, G., Mancini, L., Vanuzzo, G., Liang, P., Marchione, D., Rosi, M., Casavecchia, P.; Balucani, N. Combined crossed-beams and theoretical study of the O(^{3}P,^{1}D) + acrylonitrile (CH_2CHCN)

reactions and implications for combustion and extraterrestrial environments. *Phys. Chem. Chem. Phys*. **2023**, *25*, 20194-20211.

(53) Becke, A.D. A new Mixing of Hartree-Fock and Local Density-Functional Theories. *J. Chem. Phys.* **1993**, 98, 1372−1377.

(54) Stephens, P. J.; Devlin, F. J.; Chabalowski, C. F.; Frisch, M. J. Ab Initio Calculation of Vibrational Absorption and Circular Dichroism Spectra Using Density Functional Force Fields. *J. Phys. Chem.* **1994**, *98*, 11623−11627.

(55) Raghavachari, K.; Binkley, J.S.; Seeger, R.; Pople, J.A. Self-Consistent Molecular Orbital Methods. 20. Basis set for correlated wave-functions. *J. Chem. Phys.* **1980**, *72*, 650-54.

(56) McLean, A.D.; Chandler, G.S. Contracted Gaussian-basis sets for molecular calculations. 1. 2nd row atoms, Z=11-18. *J. Chem. Phys.* **1980**, *72*, 5639-5648.

(57) Dunning T.H. Gaussian basis sets for use in correlated molecular calculations. I. The atoms boron through neon and hydrogen *J. Chem. Phys.* **1989**, *90*, 1007–1023.

(58) Woon D.E.; Dunning T.H. Gaussian basis sets for use in correlated molecular calculations. III. The atoms aluminum through argon. *J. Chem. Phys.* **1993**, *98*, 1358–1371.

(59) Kendall, R.A.; Dunning, T.H.; Harrison, R.J. Electron affinities of the first-row atoms revisited. Systematic basis sets and wave functions. *J. Chem. Phys.* **1992**, *96*, 6796–6806.

(60) Gonzalez, C.; Schlegel, H. B. An Improved Algorithm for Reaction Path Following. *J. Chem. Phys*. **1989**, *90*, 2154−2161.

(61) Gonzalez, C.; Schlegel, H. B. Reaction Path Following in Mass-Weighted Internal Coordinates. *J. Phys. Chem*. **1990**, *94*, 5523−5527.

(62) Moore C. E. Atomic Energy Levels; National Bureau of Standards U.S. Circ. No. 467; U.S. GPO: Washington, DC, **1949.**

(63) Martin, J.M. Ab initio total atomization energies of small molecules-towards the basis set limit, *Chem. Phys. Lett*. **1996**, *259*, 669–678.

(64) Frisch, M. J.; Trucks, G. W.; Schlegel,H. B.; Scuseria,G. E.;Robb, M. A.; Cheeseman,J. R.; Scalmani,G.; Barone, V.; Mennucci,B.; Petersson,G. A.; *et al.* Gaussian09, rev. A.02; Gaussian, Inc.: Wallingford, CT, **2009.**

(65) Werner H.J; Knowles, P.J.; Knizia, *et al.* MOLPRO, version 2012.1, A package of ab initio programs, Cardiff University, Cardiff, UK, http://www.molpro.net, **2012.**

(66) Werner H.J; Knowles, P.J. *et al.* The Molpro quantum chemistry package, *J. Chem. Phys* **2020**, *152*, 144107.

(67) Hanwell, M.D.; Curtis, D.E.: Lonie, D.C.; Vandermeersch, T.; Zurek, E.; Hutchison, G.R. Avogadro: an advanced semantic chemical editor, visualization, and analysis platform *J. Cheminf*. **2012**, *4*, 17.

(68) Skouteris, D.; Balucani, N.; Faginas-Lago, N.; Falcinelli, S.; Rosi, M. Dimerization of methanimine and its charged species in the atmosphere of Titan and interstellar/cometary ice analogs. *Astron. Astrophys*. **2015**, *584*, A76.

(69) Gilbert, R.G.; Smith, S.C. Theory of unimolecular and recombination reactions, Blackwell Scientific Publications, Oxford, U.K, **1990**.

(70) Klippenstein, S.J. Variational optimizations in the Rice-Ramsperger-Kassel-Marcus theory calculations for unimolecular dissociations with no reverse barrier. *J. Chem. Phys* **1992**, *96*, 367–371.

(71) Casavecchia, P.; Leonori, F.; Balucani, N. Reaction dynamics of oxygen atoms with unsaturated hydrocarbons from crossed molecular beam studies: primary products, branching ratios and role of intersystem crossing. *Int. Rev. Phys. Chem.* **2015**, *34*, 161-204.

(72) Pan, H.; Liu, K.; Caracciolo, A.; Casavecchia, P. Crossed beam polyatomic reaction dynamics: recent advances and new insight. *Chem. Soc. Rev.* **2017**, *46*, 7517-7547.

(73) Caracciolo, A.; Vanuzzo, G.; Balucani, N.; Stranges, D.; Casavecchia, P.; Pratali Maffei, L.; Cavallotti, C. Combined experimental and theoretical studies of the O(^{3}P) + 1-butene reaction dynamics: primary products, branching fractions and role of intersystem crossing. *J. Phys. Chem. A* **2019**, *123*, 9934-9956.

(74) Vanuzzo, G.; Balucani, N.; Leonori, F.; Stranges, D.; Nevrly, V.; Falcinelli, S.; Bergeat, A.; Casavecchia, P.; Cavallotti, C. Reaction dynamics of O(^{3}P) + propyne: I. primary products, branching ratios, and role of intersystem crossing from crossed molecular beam experiments. *J. Phys. Chem. A* **2016**, *120*, 4603-4618.

(75) Alagia, M.; Aquilanti, V.; Ascenzi, D.; Balucani, N.; Cappelletti, D.; Cartechini, L.; Casavecchia, P.; Pirani, F.; Sanchini, G.; Volpi, G. G. Magnetic analysis of supersonic beams of atomic oxygen, nitrogen, and chlorine generated from a radio-frequency discharge. *Isr. J. Chem.* **1997**, *37*, 329-342.

(76) Casavecchia, P.; Leonori, F.; Balucani, N.; Petrucci, R.; Capozza, G.; Segoloni, E. Probing the dynamics of polyatomic multichannel elementary reactions by crossed molecular beam experiments with soft electron-ionization mass spectrometric detection. *Phys. Chem. Chem. Phys.* **2009**, *11*, 46-65.

(77) Chen, H.-F.; Liang, C.-W.; Lin, J. J.; Lee, Y.-P.; Ogilvie, J. F.; Xu, Z. F.; Lin, M. C. Dynamics of Reactions O(^{1}D) + C_6H_6 and C_6D_6. *J. Chem. Phys.* **2008**, *129*, 174303.

(78) Vuitton, V.; Yelle, R. V.; Klippenstein, S. J.; Hörst, S. M.; Lavvas, P. Simulating the density of organic species in the atmosphere of Titan with a coupled ion-neutral photochemical model. *Icarus* **2019**, *324*, 120–197.

(79) Miller, W. B.; Safron, S. A.; Herschbach, D. R. Exchange reactions of alkali atoms with alkali halides: a collision complex mechanism. *Discuss. Faraday Soc.* **1967**, *44*,108-123.

(80) Schmoltner, A. M.; Chu, P. M.; Lee, Y. T. Crossed molecular beam study of the reaction $O(^3P)$ + C_2H_2. *J. Chem. Phys.* **1989**, *91*, 5365-5373.

(81) Pannacci, G.; Vanuzzo, G.; Balucani, N.; Casavecchia, P. Crossed molecular beam studies of bimolecular reactions of atomic oxygen with nitrogen-bearing organic molecules (nitriles and N-heterocyclic). *Rendiconti Lincei, Scienze Fisiche e Naturali* **2024**, *35*, 1–23.

(82) Balucani, N.; Pacifici, L.; Skouteris, D.; Caracciolo, A.; Casavecchia, P.; Falcinelli, S.; Rosi, M. A computational study of the reaction $N(^2D)$ + C_6H_6 leading to pyridine and phenylnitrene. *Lecture Notes in Computer Science (LNCS)* **2019**, *11621*, 316-324.

(83) Chin, C.-H.; Zhu, T.; Zhang, J. Z. H. Cyclopentadienyl radical formation from the reaction of excited nitrogen atoms with benzene: a theoretical study. *Phys. Chem. Chem. Phys.* **2021**, *23*, 12408-12420.

(84) Lavvas, P.; Galand, M.; Yelle, R. V.; Heays, A. N.; Lewis, B. R.; Lewis, G. R.; Coates, A. J. Energy deposition and primary chemical products in Titan's upper atmosphere. *Icarus* **2011**, *213*, 233-251.

(85) Soorkia, S.; Taatjes, C. A.; Osborn, D. L.; Selby, T. M.; Trevitt, A. J.; Wilson, K. R.; Leone, S. R. Direct detection of pyridine formation by the reaction of CH (CD) with pyrrole: a ring expansion reaction. *Phys. Chem. Chem. Phys.* **2010**, *12*, 9750-9759.

(86) Holzmeier, F.; Wagner, I.; Fischer, I.; Bodi, A.; Hemberger, P. Pyrolysis of 3-methoxypyridine. Detection and characterization of the pyrrolyl radical by threshold photoelectron spectroscopy. *J. Phys. Chem. A* **2016**, *120*, 4702−4710.

(87) Zhang, Y.-R.; Yuan, D.-F.; Wang, L.-S. Probing the electronic structure and spectroscopy of pyrrolyl and imidazolyl radicals using high-resolution photoelectron imaging of cryogenically cooled anions. *Phys. Chem. Chem. Phys.* **2022**, *24*, 6505-6514.

(88) Cavallotti, C.; De Falco, C.; Maffei, L. P.; Caracciolo, A.; Vanuzzo, G.; Balucani, N.; Casavecchia, P. A theoretical study of the extent of intersystem crossing in the $O(^3P)$ + C_6H_6 reaction with experimental validation. *J. Phys. Chem. Lett.* **2020**, *11*, 9621−9628.

(89) Vanuzzo, G.; Caracciolo, A.; Minton, T. K.; Balucani, N.; Casavecchia, P.; de Falco, C.; Baggioli, A.; Cavallotti, C. Crossed-beams and theoretical studies of the $O(^3P, ^1D)$ + benzene reactions: primary products, branchingfFractions, and role of intersystem crossing. *J. Phys. Chem. A* 2021, *125*, 8434-8453.

(90) Balucani, N.; Vanuzzo, G.; Recio, P.; Caracciolo, A.; Rosi, M.; Cavallotti, C.; Baggioli, A.; Della Libera, A.; Casavecchia, P. Crossed molecular beam experiments and theoretical simulations on the multichannel reaction of toluene with atomic oxygen. *Faraday Discuss.* **2024**, in press; DOI: 10.1039/d3fd00181d

Graphical ABSTRACT